

# STELLARATOR DESIGN AND OPTIMIZATION

## A NOVEL APPROACH BASED ON VARIATIONAL PRINCIPLES

**EPFL**



Thèse présentée le 27 août 2023  
à la Faculté des sciences de base  
Swiss Plasma Center (SPC)

École polytechnique fédérale de Lausanne

pour l'obtention du grade de Physicien  
par

Salomon Guinchard

sous la direction de :

Dr. S. R. Hudson

Dr. J. Loizu

Dr. J.P. Hogge

Princeton NJ, 2023



"La vie est un gros gâteau, avec des tranches de réalité et des tranches de rêve.  
Ce sont ces dernières que j'avale avec le plus d'appétit."  
— Pierre Richard



# Acknowledgements

I would like to warmly thank my supervisor, Stuart Hudson, for making this work possible. I really appreciated you being available all semester long, always happy to reply to my questions. I want to thank you a lot for having introduced me to the stellarator community too. I would also like to thank my other advisor Joaquim, for giving me the opportunity to come to Princeton to do this work. Also, thank you Elizabeth, for taking the time to answer all my questions when I was stuck, and for making yourself available whenever I needed help. Thank you too, Wrick, for making work so fun with all your great anecdotes. I really appreciated working with you and look forward to collaborating with you again. I also want to thank my parents, and my sister, for believing in me from the start till the end. Your encouragements have helped me go through this long academic journey. Thank you to my friends Kent, Baptiste and Hugo, for all the laughter and the moments we shared during these many years spent at EPFL together. Melanie, thank you very much for being here, supporting me even when the motivation was not there. You have helped me a lot, and this experience would not have been the same without you. Finally, I would like to thank all my friends from PPPL, Vinícius, Ivan, Galina, Maté, Nikita, Pallavi, Priya and Julien, for having welcomed me warmly in the group, and made me one of yours. I will miss our post-lunch coffee break.

*Princeton, August 27, 2023*

S. G.



# Acronyms

<b>DOF</b>	degree of freedom
<b>EL</b>	Euler-Lagrange
<b>JVP</b>	jacobian vector product
<b>L-BFGS-B</b>	limited memory Broyden–Fletcher–Goldfarb–Shanno algorithm
<b>MHD</b>	magnetohydrodynamics
<b>ODE</b>	ordinary differential equation
<b>PDE</b>	partial differential equation
<b>QA</b>	quasi-axisymmetric
<b>SIMSOPT</b>	Simons stellarator optimizer code
<b>SPEC</b>	stepped-pressure equilibrium code
<b>VMEC</b>	variational moments equilibrium code
<b>VJP</b>	vector jacobian product
<b>W7X</b>	Wendelstein-7-X
<b>3D</b>	3-dimensional



# Contents

<b>Acknowledgements</b>	<b>v</b>
<b>Acronyms</b>	<b>i</b>
<b>Introduction</b>	<b>1</b>
0.1 The need for a new source of energy . . . . .	1
0.2 The stellarator: a nuclear fusion reactor or interest . . . . .	2
0.3 Outline of this thesis . . . . .	4
<b>1 Mathematical fundamentals</b>	<b>5</b>
1.1 Floquet theory . . . . .	5
1.2 Shape optimization . . . . .	6
1.2.1 General formalism . . . . .	6
1.2.2 Volume-integrated functionals . . . . .	8
1.2.3 Curve-integrated functionals . . . . .	8
<b>2 Towards an Euler-Lagrange equation for an optimized stellarator</b>	<b>11</b>
2.1 Requirements for a basic stellarator . . . . .	11
2.2 Fixed boundary optimization . . . . .	12
2.3 Coils construction . . . . .	16
2.4 Summary . . . . .	16
<b>3 Floquet theory and calculus of variations</b>	<b>17</b>
3.1 First variation of the magnetic action . . . . .	17
3.2 Second variation and Floquet theory . . . . .	18
3.3 Consistency verifications: Mercier coordinates . . . . .	19
3.3.1 The second variation of the action in Mercier coordinates . . . . .	19
3.3.2 Imposing constraints from MHD . . . . .	21
3.3.3 Floquet exponents and rotational transform . . . . .	22
3.4 Floquet exponents from infinite Hill's determinant . . . . .	26
3.4.1 The second variation of the action in Solovev-Shafranov coordinates	26
3.4.2 Floquet exponents and the Hill's determinant . . . . .	30
3.4.3 Summary . . . . .	34
3.5 Discrete formalism: piecewise action . . . . .	35

## Contents

---

3.5.1	Particular case: piecewise linear . . . . .	38
3.6	Conclusion . . . . .	39
<b>4</b>	<b>Coil vacuum energy to reduce inter-coil forces</b>	<b>41</b>
4.1	The energy functional . . . . .	41
4.2	The Simsopt code . . . . .	44
4.2.1	Functional optimization . . . . .	44
4.2.2	L-BFGS-B algorithm and Jacobian vector product . . . . .	45
4.3	Pseudo-energy minimization . . . . .	45
4.3.1	Target functional . . . . .	45
4.3.2	Limitations to the filamentary coil description . . . . .	46
4.4	Implementation verifications and consistency checks . . . . .	48
4.4.1	Behavior as a function of the ghost-curve . . . . .	48
4.4.2	Increasing the penalty on the energy . . . . .	50
4.5	Results . . . . .	52
4.5.1	Precise QA configuration . . . . .	52
4.5.2	The W7X configuration . . . . .	54
4.5.3	Summary . . . . .	55
<b>5</b>	<b>Conclusion and futures perspectives</b>	<b>57</b>
5.1	Future perspectives . . . . .	57
<b>A</b>	<b>Appendices</b>	<b>59</b>
A.1	Derivation of the transport theorems . . . . .	59
A.2	Tangential differential operators . . . . .	62
A.3	Shape-gradient derivations of volume and area . . . . .	63
A.4	Derivation of the first variation of the magnetic action . . . . .	64
A.5	Frenet-Serret frame . . . . .	65
A.6	Vector Jacobian products . . . . .	66
	<b>Bibliography</b>	<b>67</b>

# Introduction

## 0.1 The need for a new source of energy

With a tremendous increase in the world population in the last decades, the demand for energy is higher than ever. Together with the increase in the population, the earth has seen its greenhouse gases concentration rise too. Fossil fuels are known to be polluting, and their daily usage in industrial and traveling sectors keeps the greenhouse gases emissions ongoing. Therefore, it appears essential to come up with an alternative to fossil fuels. For an economical model to be based on this new source of energy, the latter would have to satisfy at least three criteria:

- Be able to satisfy the high demand.
- Be less polluting than fossil fuels.
- Be affordable enough to be used worldwide.

A promising alternative, that emerged in the 1950's, is *nuclear fusion*. Nuclear fusion is the nuclear reaction that occurs in the core of stars, where the temperature and density conditions, due to the gravitational field are convenient for fusion to happen. One of the obstacles in reproducing this reaction of earth is that the pressure and density conditions make fusion unlikely to happen spontaneously. Therefore, we need to come up with a device in which such a reaction is possible, being able to heat the fusion material to extremely high temperatures, and sustain these conditions for a long-enough time to produce energy for a worldwide demand. Nuclear fusion is promising because of its very high energy density, in fact, approximately  $10^7$  times higher than the combustion of gasoline (Imbert-Gerard et al. (2020)).

In magnetically-confined nuclear fusion, two classes of reactors exist: Tokamaks, and Stellarators. Fig.(1) illustrates the two concepts. The Tokamak concept is an axisymmetric toroidal device, in which the magnetic field for confinement is achieved by mean of a combination of external magnetic coils and a plasma current. However, it is

## Introduction

---

known that the plasma current can drive instabilities and chaos, by opening magnetic islands for example. See Fig.(2). However, the Stellarator concept is a 3D confinement device, in which the magnetic field is purely externally generated. A brief introduction to stellarators feature will be given in the next section, and the interested reader can read through Boozer (1998) and Imbert-Gerard et al. (2020).

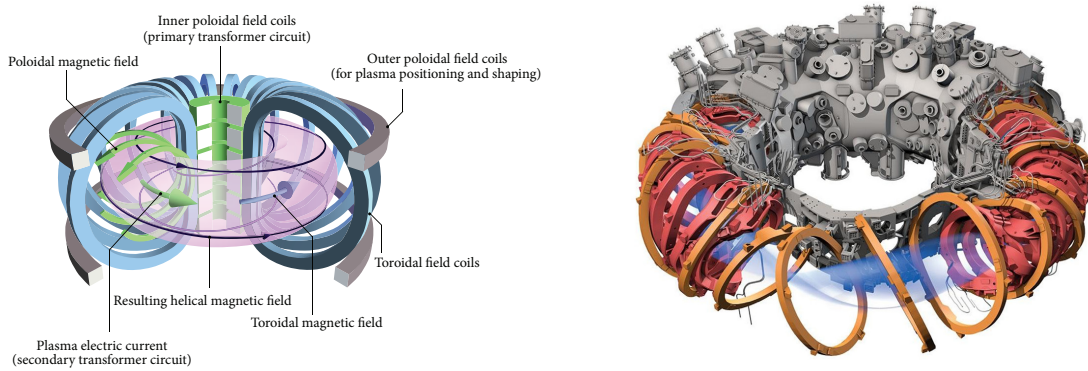


Figure 1 – Left: Schematics of a Tokamak Li et al. (2014)- Right: The stellarator W7X Klinger et al. (2019)

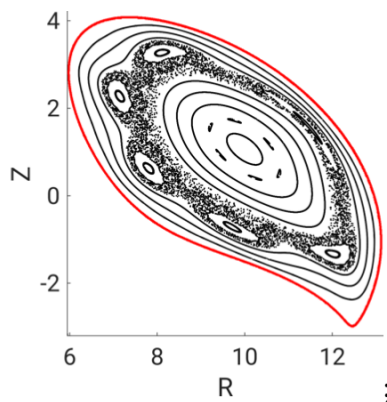


Figure 2 – Stellarator Poincaré section with magnetic islands. Figure reproduced from Baillod (2023) with authorization.

## 0.2 The stellarator: a nuclear fusion reactor or interest

As stated earlier, stellarators are 3D confinement devices, for which the field is solely generated by external coils. The downside of that is that the geometry is much more complicated, making stellarator configurations very difficult to optimize for. A great

## 0.2. The stellarator: a nuclear fusion reactor or interest

---

advantage is that stellarators do not have current driven instabilities present in tokamaks, making them more stable. Moreover, stellarators can be operated in steady-state, whereas tokamaks need to be operated in pulse mode.

A physical parameter of interest in order to achieve good confinement of particles in stellarators in the rotational transform, denoted  $\iota$ . Iota corresponds to the number of poloidal rotations achieved by a magnetic field line per toroidal period, and can be expressed by the following expression:

$$\iota := \frac{\mathbf{B} \cdot \nabla\theta}{\mathbf{B} \cdot \nabla\phi} \Big|_{\mathbf{B}}, \quad (1)$$

where  $\theta$  denotes the poloidal angle and  $\phi$  the toroidal angle. Moreover, the on-axis rotational transform is of interest. From Mercier's expression Mercier et al. (1987), the on-axis rotational transform takes the following form

$$\iota_a = \oint \frac{ds}{\cosh\eta} \left( \frac{J_0}{2B_0} + \delta' + \frac{1}{T} \right), \quad (2)$$

where  $J_0$  is the current density,  $\delta$  controls the rotation of flux surfaces and  $1/T$  the torsion of the magnetic axis. Therefore, one sees that  $\iota$  can be induced by three ways: rotating the elliptical surfaces around the magnetic axis, by bending the magnetic axis to give it torsion, or by inducing a current in the plasma (see Fig(3)).

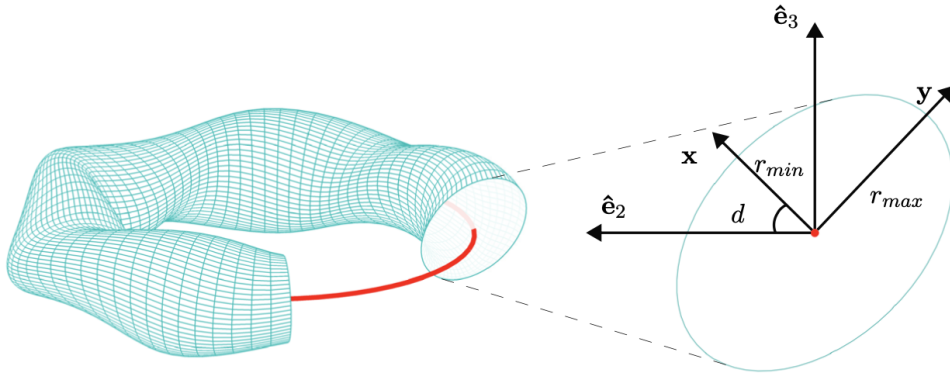


Figure 3 – Elliptical flux surface rotating around a toroidal axis (in red) - Figure reproduced from Baillod (2023) with authorization.

Therefore, since  $\iota_a$  is such an important parameter, it is essential that it is computed accurately. In this thesis, we come up with a formalism to compute the rotational transform, as well as with a novel approach to design the coils for stellarator configurations.

### 0.3 Outline of this thesis

This thesis aims at setting the bases of what is needed to generalize the framework of stellarator optimization. Necessary mathematical tools are given in chapter 1. The requirements for a basic stellarator are introduced in chapter 2, in which we attempt to write an Euler Lagrange equation for an optimized stellarator. If one were to be provided with such an equation, it might be easier to map the space of optimized configurations, since they would be located at extremal configurations with respect to that EL equation. Defining such an equation is challenging and require some "ingredients", and in addition, for them to be all brought into the same (surface-)variational form. One of them, the on-axis rotational transform  $\tau_a$ , is a curve-integrated property, which curve is dependent on the surface enclosing a toroidal volume, making it difficult to write the terms in the correct form. The link between periodic curves and Floquet theory, and how it is used to compute  $\tau_a$ , is made in chapter 3. In this same chapter, a new method to compute numerically  $\tau_a$  is also introduced. Finally, optimizing for a stellarator needs to design optimal coils. A novel approach in the design of those coils is given in chapter 4.

# 1 Mathematical fundamentals

Let us start this thesis with a brief chapter dedicated to the mathematical fundamentals required for what will follow. We start by introducing the main results from Floquet theory, which will be essential to recover the rotational transform  $\iota$ . The second section is dedicated to shape optimization, relevant here since both the surface and the coils are objects for which we will attempt to optimize for.

## 1.1 Floquet theory

Floquet theory was formulated by Gaston Floquet towards the end of the 19th century, in his attempt to solve linear differential equations with periodic coefficients (see Floquet (1883)). The basics of the Floquet formalism can be formulated starting from the following problem. Suppose one needs to solve the linear system,

$$\dot{\mathbf{x}} = A(t)\mathbf{x} \quad \mathbf{x}(t_0) = \mathbf{x}_0, \tag{1.1}$$

where  $A \in \mathcal{M}_{n \times n}$  is periodic in  $t$  with period  $T$ . Considering  $n$  solutions of Eq.(1.1)  $\{\mathbf{x}_1, \dots, \mathbf{x}_n\}$ , it is useful to rewrite the system in the form of a matrix equation, defining the so-called fundamental matrix  $X$  by grouping the  $\mathbf{x}_i$  together

$$X(t, t_0) := \begin{pmatrix} \mathbf{x}_1; \mathbf{x}_2; \dots; \mathbf{x}_n \end{pmatrix}$$

where the second argument has been added to specify that the initial condition occurs at time  $t_0$ . Thus, Eq.(1.1) can be rewritten as

$$\frac{d}{dt}X(t, t_0) = A(t)X(t, t_0), \quad X(t_0, t_0) = \mathbb{I}. \tag{1.2}$$

We now state a few results that will be useful later on.

**Theorem (Abel).** The determinant of the fundamental matrix  $X$  is

$$\det(X(t, t_0)) = \exp \int_{t_0}^t \text{tr}A(s)ds. \quad (1.3)$$

Moreover, it can be rewritten as the product of the so-called *Floquet multipliers*

$$\det(X(t, t_0)) = \prod_{i=1}^n e^{\lambda_i T}, \quad (1.4)$$

where the  $\lambda_i$  are the Floquet exponents, which will be shown to be linked with the rotational transform. The proof of the above theorem can be found in Meiss (2007). The second statement implies that the Floquet multipliers are the eigenvalues of the fundamental matrix of the linear system Eq.(1.2).

Now we state the main result of the Floquet theory:

**Theorem (Floquet-Lyapunov).** The fundamental matrix  $X$  solution of the system Eq.(1.2) is of the form

$$X(t, 0) = P(t)e^{tB} \quad (1.5)$$

where the matrix  $P$  is symplectic and  $T$ -periodic, and  $B$  is a constant hamiltonian matrix. Here again, a proof can be found in Meiss (2007). This last result is very important since it will enable us to link Floquet theory with the variational calculus carried on the magnetic action in chapter 3. What has been introduced previously is enough for our problem, but for more on Floquet theory, the author recommends Meiss (2007) and Floquet (1883).

## 1.2 Shape optimization

### 1.2.1 General formalism

We follow Laurain and Sturm (2015), Delfour and Zolésio (2011) to introduce the mathematical fundamentals of the shape-optimization formalism, necessary here since it will be our base to construct coils from minimizing certain functionals, as well as to motivate the introduction of an Euler-Lagrange equation for an optimized stellarator.

Let us start with the notation that we'll use. We denote by  $\mathcal{P}(D)$  the set of subsets of  $D \subset \mathbb{R}^d$ , compactly contained in  $\mathbb{R}^d$ , with  $D$  assumed to be open and bounded. Now, for  $k \geq 0$  and  $0 \leq \alpha \leq 1$ ,

$$C_c^{k,\alpha} := \left\{ \Theta \in C^{k,\alpha} \left( D, \mathbb{R}^d \right) \mid \Theta \text{ has compact support in } \mathbb{R}^d \right\}. \quad (1.6)$$

Let  $\Theta \in C_c^{0,1} (D, \mathbb{R}^d)$  denote a vector field. To the latter, it is possible to associate the following flow:

**Definition.** *Eulerian flow.* The vector field  $\Phi_\epsilon^\Theta : \bar{D} \rightarrow \mathbb{R}^d$ , with  $\epsilon \in [0, \epsilon_0]$ , is defined for each  $x_0 \in \bar{D}$  as  $\Phi_\epsilon^\Theta(x_0) := x(t)$  where  $x : [0, \epsilon_0] \rightarrow \mathbb{R}^d$  solves

$$x'(\epsilon) = \Theta(x(\epsilon)) \quad \text{for } \epsilon \in (0, \epsilon_0), \quad x(0) = x_0. \quad (1.7)$$

Now, let  $J : \mathcal{B} \rightarrow \mathbb{R}$  denote a shape-functional defined on some 'good'  $\mathcal{B}$ :

**Definition.** *Eulerian semiderivative.* The eulerian semiderivative of  $J$  at  $\Omega$  in the direction  $\Theta \in C_c^{0,1} (D, \mathbb{R}^d)$ , is defined, if the limit exists, as

$$dJ(\Omega)(\Theta) := \lim_{\epsilon \downarrow 0} \frac{J(\Omega_\epsilon) - J(\Omega)}{\epsilon}, \quad (1.8)$$

where  $\Omega_\epsilon := \Phi_\epsilon^\Theta(\Omega)$ , with  $\Phi_\epsilon^\Theta$  the eulerian flow associated with the vector field  $\Theta$ . The functional  $J$  is said to be *shape-differentiable* at  $\Omega$  if it has an eulerian semiderivative at  $\Omega$  for all  $\Theta \in C_c^\infty (D, \mathbb{R}^d)$  and the mapping

$$dJ(\Omega) : C_c^\infty (D, \mathbb{R}^d) \rightarrow \mathbb{R}, \quad \Theta \mapsto dJ(\Omega)(\Theta) \quad (1.9)$$

is linear and continuous, in which case  $dJ(\Omega)(\Theta)$  is called *shape derivative* at  $\Omega$ .

The previous definitions were crucial in that they are necessary to introduce the central theorem of shape-optimization, the Hadamard-Zolésio structure theorem, which will be the starting point to motivate an Euler-Lagrange equation for an optimized stellarator, or else when optimizing coils shapes to recover a target surface.

**Theorem. Structure theorem. (Hadamard - Zolésio).** Assume  $\Gamma := \partial\Omega$  is compact, and  $J$  is shape-differential in the sense of the previous definition. Denoting the shape derivative by

$$dJ(\Omega) : C_c^\infty (D, \mathbb{R}^d) \rightarrow \mathbb{R}, \quad \Theta \mapsto dJ(\Omega)(\Theta). \quad (1.10)$$

Assuming  $dJ$  to be of order  $k \geq 0$ , and  $\Gamma$  of class  $C^{k+1}$ , then there exists a linear and continuous functional  $g : C^k(\Gamma) \rightarrow \mathbb{R}$  such that

$$dJ(\Omega)(\Theta) = g(\Theta|_\Gamma \cdot n), \quad (1.11)$$

with  $\Theta|_\Gamma$  the restriction of  $\Theta$  to the boundary and  $n$  the unit normal to that boundary. A proof can be found in Delfour and Zolésio (2011).

This theorem is essential in the sense that it ensures the possibility to write down shape

functionals variations in a shape-gradient form, where the variation is expressed as an integral of a shape-gradient projected onto the normal of the domain of integration. This result is exploited in the formalism described in 2.1, as well as in Eq.(1.15).

### 1.2.2 Volume-integrated functionals

We want to express the variation of a volume integrated functional in a shape-gradient form similar to Eq.(1.11). Take the volume integrated functional

$$\mathcal{F} := \int_{\mathcal{V}} f \, dV \quad (1.12)$$

Then by the structure theorem, one can write the variation  $\delta\mathcal{F}$  in the form

$$\delta\mathcal{F} = \int_S \mathcal{G}_{\mathcal{F}}(\delta\boldsymbol{\sigma} \cdot \mathbf{n}) \, dS \quad (1.13)$$

where  $S = \partial\mathcal{V}$  is parametrized by  $\boldsymbol{\sigma}$  with  $\mathbf{n}$  as unit normal, and  $\mathcal{G}_{\mathcal{F}}$  the shape-gradient of  $\mathcal{F}$ .

### 1.2.3 Curve-integrated functionals

Similar results can be derived for curve-integrated functionals. Take a functional  $f$  that depends on integration along a set of closed curves  $\{C_i\}$ .

$$f = \sum_{i=1}^{N_c} \oint_{C_i} dl \, f_i \quad (1.14)$$

It is possible to write its first variation with respect to a change in the curves parametrization  $\{\delta\mathbf{x}_i\}$ . Since tangential variations, at first order, will not contribute in the change of the integrated functional, it is possible to represent the shape derivative of  $f$  in a shape gradient form:

$$\delta f[\{\delta\mathbf{x}_i\}] = \sum_i \oint_{C_i} dl \, (\delta\mathbf{x}_i \times \mathbf{t}) \cdot \mathcal{G}_i, \quad (1.15)$$

where  $\mathcal{G}_i$  is the shape gradient of  $f$  with respect to a variation in the  $i$ -th curve geometry. Note that  $\mathcal{G}_i$  is a vector, and it characterizes the sensitivity of  $f$  to variations that are normal to the  $i$ -th curve.

Exploiting properties of the triple product, it is possible to rewrite Eq.(1.15) as

$$\delta f[\{\delta\mathbf{x}_i\}] = \sum_i \oint_{C_i} dl \, \tilde{\mathcal{G}}_i \cdot \delta\mathbf{x}_i, \quad (1.16)$$

## 1.2. Shape optimization

---

where  $\tilde{\mathcal{G}}_i$  is analogous to the shape gradient  $\mathcal{G}_i$ , except that it characterizes the sensitivity of the functional with respect to a change in the curves geometries, no matter what the direction considered, whereas  $\mathcal{G}_i$  accounts for the sensitivity to changes normal to the curves.

Assume now that the curves are described by a set of parameters  $\{\Omega_i^k\}$ , say the Fourier modes in their Fourier series representation. Then it is possible to express the variation of the functional  $f$  with respect to a change in the curves geometries through derivatives with respects to the  $\{\Omega_i^k\}$ . Using that (with Einstein's summation convention)

$$\delta f[\{\delta\Omega_k\}] = \frac{\partial f}{\partial\Omega_k} \delta\Omega_k \quad \text{and} \quad \delta\mathbf{x}_i[\{\delta\Omega_k\}] = \frac{\partial\mathbf{x}_i}{\partial\Omega_k} \delta\Omega_k \quad (1.17)$$

one easily obtains the following for  $\delta f$ ,

$$\begin{aligned} \delta f &= \sum_i \oint_{C_i} dl \tilde{\mathcal{G}}_i \cdot \delta\mathbf{x}_i \\ &= \sum_{i,k} \oint_{C_i} dl \left( \tilde{\mathcal{G}}_i \cdot \frac{\partial\mathbf{x}_i}{\partial\Omega_k} \right) \delta\Omega_k \\ &= \sum_{i,k} \oint_{C_i} dl \left( \frac{\partial\mathbf{x}_i}{\partial\Omega_k} \times \mathbf{t} \right) \cdot \mathcal{G}_i \delta\Omega_k \end{aligned} \quad (1.18)$$

which enables to identify the parameter derivatives for  $f$ :

$$\frac{\partial f}{\partial\Omega_k} = \sum_i \oint_{C_i} dl \left( \frac{\partial\mathbf{x}_i}{\partial\Omega_k} \times \mathbf{t} \right) \cdot \mathcal{G}_i, \quad (1.19)$$

or else using the pseudo shape-gradient  $\tilde{\mathcal{G}}$  expression:

$$\frac{\partial f}{\partial\Omega_k} = \sum_i \oint_{C_i} dl \tilde{\mathcal{G}}_i \cdot \frac{\partial\mathbf{x}_i}{\partial\Omega_k}. \quad (1.20)$$

Now that shape-gradient results and parameter derivatives have been introduced for curve-integrated functionals, we are equipped with all the tools needed to delve into the problem of stellarator design.



## 2 Towards an Euler-Lagrange equation for an optimized stellarator

As it has been stated in the introduction to this thesis, a stellarator is a magnetic field configuration that shows promises for fusion energy. Let us now delve in more details on a new approach to design such a magnetic configuration. In section 2.1, the requirements to construct a basic stellarator field are stated. The problem is divided into two subproblems. The first one is dealt with in section 2.2, whereas the second one is introduced in section 2.3, but will be treated in more details in chapter 4 since we bring in a novel approach to construct the coils.

### 2.1 Requirements for a basic stellarator

In order for a vacuum magnetic field to define a (basic) stellarator, several properties are required:

- A toroidal bounded region of space  $\mathcal{V}$  with non-zero volume  $V$ .
- A flux surface  $S$  such that (for the sake of simplicity)  $S = \partial\mathcal{V}$  and  $\mathbf{B} \cdot \mathbf{n} = 0$  on  $S$ .
- Non-zero toroidal flux  $\Psi > 0$ .
- Non-zero on-axis rotational transform.

Taking the previous requirements into consideration, one can formulate the following problem. Given a certain value for  $V$ , and a certain on-axis rotational transform  $\tau_a$ , what boundary  $S = \partial\mathcal{V}$  minimizes the inter-coil forces? Since the previously stated problem involves finding a surface that minimizes a given quantity, for an appropriately defined functional  $\mathcal{F}[S]$ , an Euler-Lagrange equation can be derived. The obtained stellarator configuration is therefore optimal w.r.t. the inter-coil forces, and no other quantity such as quasi-symmetry is targeted. However, in what follows, to be consistent with terminology involving Euler-Lagrange equations and optimization, we'll use the term *optimized-stellarator*.

## Chapter 2. Towards an Euler-Lagrange equation for an optimized stellarator

---

The above problem for an optimized stellarator can then be divided in two sub-problems:

1. Fixed boundary problem: given  $V$  and  $\tau_a$ , find  $S$  that minimizes the internal energy  $\mathcal{E}_I$ .
2. Given  $S$ , construct a set of coils with minimal forces.

### 2.2 Fixed boundary optimization

Let us focus on the first problem, that is to find the surface given  $V$  and  $\tau_a$ . Therefore, the degree of freedom is  $S$ . Both the volume  $V[S]$  and the area  $A[S]$  are functionals that can be expressed as functions of  $S$ . We require that the magnetic field is tangent to the surface, that is  $\mathbf{B} \cdot \mathbf{n} = 0$  on  $S$ , and we enforce a constraint on the toroidal flux,  $\Psi$ . Given the two previous constraints, one then solves for  $\mathbf{B}$  either by using a scalar or a vector potential:

$$\begin{aligned}\mathbf{B} &= \nabla\Phi \quad \text{then solve } \nabla \cdot \nabla\Phi = 0, \quad \text{or} \\ \mathbf{B} &= \nabla \times \mathbf{A} \quad \text{then solve } \nabla \times \nabla \times \mathbf{A} = 0.\end{aligned}\tag{2.1}$$

The internal magnetic energy  $\mathcal{E}_I$  can then be computed from  $\mathbf{B}$  with

$$\mathcal{E}_I := \frac{1}{2\mu_0} \int_V B^2 dV,\tag{2.2}$$

and since the magnetic axis can be identified, the on-axis rotational transform can be computed. From now on, the terminology *Floquet-exponent* will be used instead of *rotational-transform*, since it will be shown later on that the rotational transform for a periodic curve can be recovered from the general Floquet theory, and that part of the purpose of this thesis is to emphasize the power of Floquet theory when applied to magnetic field lines. Note that given the magnetic axis parametrized by  $\mathbf{x}_a$ , it is related to the Floquet exponent of nearby trajectories by

$$\mathbf{x} := \mathbf{x}_a + e^{\lambda\zeta} \mathbf{v},\tag{2.3}$$

where  $\lambda$  is the Floquet exponent,  $\zeta$  an appropriate toroidal angle, and  $\mathbf{v}$  the direction of displacement from the axis for the nearby trajectory in question. This will be treated in more details in chapter 3, where  $\lambda$  will be determined from the second variation of the magnetic field-line action, and as of now, all that one has to remember is that there is a one-to-one mapping between  $\lambda$  and  $\tau_a$ .

Now that the problem and the terms involved have been properly stated and introduced, we propose to optimize for the surface by minimizing the internal energy, constraining the rotational transform and the volume. Therefore, one can define the following functional

## 2.2. Fixed boundary optimization

---

to minimize:

$$\mathcal{F}[S] := \mathcal{E}_I + v(V - V_0) + m(\lambda - \lambda_0), \quad (2.4)$$

where  $V_0$  and  $\lambda_0$  are the constrained volume and Floquet-exponent, and  $v$  and  $m$  are the associated Lagrange multipliers. Note that the surface can be pathological in the sense that it might have an infinite area  $A[S]$ , but still enclose a finite volume. Such fractal surfaces can be formed by a toroidal rotation of an infinitely long curve enclosing a finite surface area, such as the Koch snowflake from Fig.(2.1), or space filling curves such as Hilbert curves. A good reference for fractal-interested readers is the book by Peitgen and Saupe (1988). In light of that, the functional  $\mathcal{F}$  has to be modified to prevent  $S$

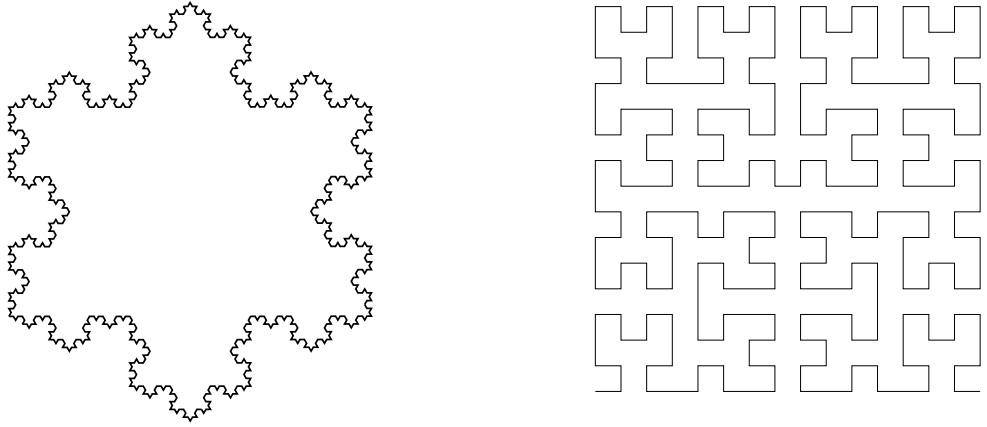


Figure 2.1 – Left: Koch snowflake. - Right: Hilbert curve of order  $n = 4$ .

from becoming fractal, by adding a penalty on the aspect ratio  $a := A^{1/2}/V^{1/3}$ ,

$$\mathcal{F}[S] := \mathcal{E}_I + \alpha a + v(V - V_0) + m(\lambda - \lambda_0). \quad (2.5)$$

Since all the previously introduced quantities can be expressed as functions of the surface parametrization  $\sigma$ , one can use the Hadamard-Zolésio theorem to ensure that the variation of  $\mathcal{F}$  w.r.t. a change in the surface parametrization  $\delta\sigma$  can be written as

$$\delta\mathcal{F}[\delta\sigma] = \int_S (\delta\sigma \cdot \mathbf{n}) \mathcal{G} dS, \quad (2.6)$$

where  $\mathcal{G}$  is the shape gradient of the functional  $\mathcal{F}$ . Therefore, by linearity, each term of  $\delta\mathcal{F}$  can be written in the shape gradient form Eq.(2.6).

1. **Volume:**

$$V := \int_{\mathcal{V}} dV, \quad \delta V = \int_S (\delta \boldsymbol{\sigma} \cdot \mathbf{n}) \, dS \quad (2.7)$$

2. **Area:**

$$A := \int_S dS, \quad \delta A = \int_S (\delta \boldsymbol{\sigma} \cdot \mathbf{n}) 2H \, dS, \quad (2.8)$$

where  $H$  is the mean curvature  $H = 1/2 \nabla_S \cdot \mathbf{n}$ . The definition and derivation of the tangential gradient operator  $\nabla_S$  can be found in appendix A.2. Derivations of Eq.(2.7)-(2.8) can be found in appendix A.3. The volume and surface variations  $\delta V$  and  $\delta A$  having been defined, one can derive the variation of the aspect ratio  $\delta a$ .

3. **Aspect ratio:**

$$\begin{aligned} \delta a &\equiv \delta (A^{1/2} V^{-1/3}) = \frac{1}{2} A^{-1/2} V^{-1/3} \delta A - \frac{1}{3} A^{1/2} V^{-4/3} \delta V \\ &= A^{-1/2} V^{-1/3} \int_S (\delta \boldsymbol{\sigma} \cdot \mathbf{n}) H \, dS - \frac{1}{3} A^{1/2} V^{-4/3} \int_S (\delta \boldsymbol{\sigma} \cdot \mathbf{n}) \, dS. \end{aligned} \quad (2.9)$$

Therefore,  $\delta a = 0 \implies H = A/3V = \text{cst}$ . Surfaces that extremize  $a$  have constant mean curvature.

4. **Internal energy:** We recall that the internal energy term is defined in Eq.(2.2). Its variation can be derived using the vector potential representation of the magnetic field  $\mathbf{B} = \nabla \times \mathbf{A}$  and the transport theorem for integrated functionals A.1:

$$\begin{aligned} \delta \mathcal{E}_I &= \int_{\mathcal{V}} \mathbf{B} \cdot \delta \mathbf{B} \, dV + \frac{1}{2} \int_S (\mathbf{B} \cdot \mathbf{B}) \delta \boldsymbol{\sigma} \cdot \mathbf{n} \, dS \\ &= \int_{\mathcal{V}} \mathbf{B} \cdot (\nabla \times \delta \mathbf{A}) \, dV + \frac{1}{2} \int_S (\mathbf{B} \cdot \mathbf{B}) \delta \boldsymbol{\sigma} \cdot \mathbf{n} \, dS \\ &= \int_{\mathcal{V}} \nabla \cdot (\delta \mathbf{A} \times \mathbf{B}) + \delta \mathbf{A} \cdot (\nabla \times \mathbf{B}) \, dV + \frac{1}{2} \int_S (\mathbf{B} \cdot \mathbf{B}) \delta \boldsymbol{\sigma} \cdot \mathbf{n} \, dS \\ &= \int_S \left\{ (\delta \mathbf{A} \times \mathbf{B}) \cdot \mathbf{n} + \frac{B^2}{2} (\delta \boldsymbol{\sigma} \cdot \mathbf{n}) \right\} \, dS, \end{aligned} \quad (2.10)$$

where we assumed that  $\nabla \times \mathbf{B} = 0$  inside  $\mathcal{V}$ , and  $\mu_0 = 1$  for the sake of readability. Now, the variation of  $\mathbf{A}$  is related to the change in the (ideal) surface through

$\delta \mathbf{A} = \delta \boldsymbol{\sigma} \times \mathbf{B}$ , enabling to write

$$\begin{aligned}\delta \mathcal{E}_I[\delta \boldsymbol{\sigma}] &= \int_S \left[ (\mathbf{B} \cdot \delta \boldsymbol{\sigma}) \mathbf{B} - B^2 \delta \boldsymbol{\sigma} \right] \cdot \mathbf{n} + \frac{B^2}{2} (\delta \boldsymbol{\sigma} \cdot \mathbf{n}) \, dS \\ &= - \int_S \frac{B^2}{2} (\delta \boldsymbol{\sigma} \cdot \mathbf{n}) \, dS.\end{aligned}\quad (2.11)$$

The only term left from the functional  $\mathcal{F}$  to compute is the variation of the Floquet term  $\lambda - \lambda_0$ .

5. **Floquet exponent:** The variation of the Floquet exponent is necessary since  $\lambda$  appears in  $\mathcal{F}$  but is difficult to compute. Indeed, it will be shown in chapter 3 that the Floquet exponent is an integral property of the magnetic axis, the latter being determined by the magnetic field inside the volume  $\mathcal{V}$  bounded by  $S$ . Therefore, if one were to compute the term  $\delta\lambda$  in a shape-gradient form analogous to the terms previously derived, one would want to express the result as follows:

$$\delta\lambda[\delta \boldsymbol{\sigma}] \equiv \delta\lambda [\delta \mathbf{x}_a[\delta \boldsymbol{\sigma}]] := \int_S \mathcal{G}_\lambda (\delta \boldsymbol{\sigma} \cdot \mathbf{n}) \, dS, \quad (2.12)$$

with  $\mathcal{G}_\lambda$  the shape gradient of  $\lambda$  with respect to a change in the surface parametrization, that is the sensitivity of  $\lambda$  to changes of  $S$ . As of now, the variation  $\delta\lambda$  can not be computed formally, since the author was not able to express the result in a shape-gradient form suitable for the Euler-Lagrange equation problem.

Therefore, an Euler-Lagrange equation can be derived, combining all the previous results:

$$\delta \mathcal{F} = \int_S \left\{ -\frac{B^2}{2} + \alpha (3V\mathcal{H} - A) + p + q\mathcal{G}_\lambda \right\} (\delta \boldsymbol{\sigma} \cdot \mathbf{n}), \quad (2.13)$$

$\mathcal{H}$  being the main curvature of  $S$ . So a surface extremizing the functional  $\mathcal{F}$  must satisfy the following EL equation:

$$-\frac{B^2}{2} + \alpha (3V\mathcal{H} - A) + p + q\mathcal{G}_\lambda = 0. \quad (2.14)$$

However, the second variation need to be investigated in order to determine the nature of the extrema, if they are local or global minima and maxima respectively. Alternatively, it might be useful to combine the previous analytical process with a numerical search of the parameter space around the extrema obtained from Eq.(2.14).

## 2.3 Coils construction

Once the surface has been optimized for, the second step in the design of our stellarator is to construct coils that will recover the surface  $S$ , and enable to minimize the quadratic flux  $\Phi_2$  with a constraint on the toroidal flux  $\Psi$ . We recall the definition of the quadratic flux:

$$\Phi_2 := \frac{1}{2} \int_S (\mathbf{B} \cdot \mathbf{n})^2 dS. \quad (2.15)$$

Therefore, it is possible to define a functional to minimize, taking into account the constraints, as we did for Eq.(2.4), as a function of the coils geometries  $\{C_i\}$ :

$$\mathcal{F}_S[\{C_i\}] := \Phi_2 + p(\Psi - \Psi_0) + \sum_j \omega_j f_j, \quad (2.16)$$

with the  $f_j$  being functions such as the average coil-to-coil separation, the mean coil curvature, or the mean coil torsion and so on. Another coils-dependent quantity can be introduced, in an attempt to minimize the inter-coils forces. The vacuum field energy, that is the integral of the squared magnetic field over all space, for example. At this point of the work, penalizing the vacuum-field energy to reduce the inter-coils forces is rather speculative, but our intuition guides us in that direction. Indeed, a conducting loop carrying an electrical current through a magnetic field undergoes a magnetostatic force. Therefore, minimizing the magnetic field outside of the toroidal volume of interest tends to let us think that coils could be constructed with less forces between them. Introducing the vacuum field energy as a new penalty is no trivial task, and hence will therefore be treated separately, in chapter 4.

## 2.4 Summary

In this chapter, we introduced the requirements for a basic stellarator. In a nutshell, we need a surface and a set of coils that wind around the latter. In our search for an Euler-Lagrange equation for an optimized stellarator, we have subdivided the problem in the two obvious parts that are optimizing for the surface and then construct a set of coils to recover the surface in question. We mentioned that the on-axis rotational transform, an essential "ingredient" for a stellarator, is linked to the Floquet exponents of the magnetic axis. In fact, in a more general case, Floquet theory can describe the behavior of periodic trajectories and hence closed field lines in other situations too, such as around an X point, but this topic is beyond the scope of this work. Then, what it takes to "construct" mathematically the coils has been introduced and we proposed to add a new feature in the optimization process, that is to attempt reducing the forces on the coils by lowering the energy. Since this requires that the vacuum field energy and its properties are properly defined, it will be treated in chapter 4, after we demonstrate in the following chapter how  $\tau_a$  is related to the Floquet exponents of the magnetic axis.

# 3 Floquet theory and calculus of variations

It has been claimed in chapter 2 that the rotational transform is linked to the Floquet exponents of the second variation of the magnetic field line action. This chapter aims at proving the above statement. In section 3.1 the magnetic action is introduced and its first variation is derived. In section 3.2, the second variation of the action is derived and the latter is expressed in the form of an operator. Section 3.4 aims at connecting the Floquet theory to the calculus of variations introducing the theory of the Hill's infinite determinant after that  $\epsilon_a$  has been recovered in section 3.3, as a consistency check. Finally, a discrete formalism is introduced to compute the Floquet exponents from a finite dimensional eigenvalue problem, as a solution to the Hill's infinite dimensional matrix, in section 3.5, which is a novel approached based on some existing work by Mackay and Meiss (1983) and Greene (2008).

## 3.1 First variation of the magnetic action

Let us start by defining the magnetic field line action. Provided a curve  $\mathcal{C}$  that will be assumed to be closed in what follows, we can define the action as the integral along  $\mathcal{C}$  of the magnetic vector potential  $\mathbf{A}$ , with  $\mathbf{B} = \nabla \times \mathbf{A}$ :

$$\mathcal{S} := \oint_{\mathcal{C}} \mathbf{A} \cdot d\mathbf{l}. \quad (3.1)$$

The first variation with respect to a change in the curve geometry  $\delta\mathbf{x}$ , is

$$\delta\mathcal{S} = \int_{\mathcal{C}} \mathbf{x}' \times \mathbf{B} \cdot \delta\mathbf{x} \, dl. \quad (3.2)$$

which shows that stationary integral curves are tangential to the magnetic field, see appendix A.4 for the derivation. In order to derive the formalism to recover the on-axis rotational transform, the second variation of the magnetic action is needed.

### 3.2 Second variation and Floquet theory

Eq.(3.2) shows that closed curves extremizing the magnetic action are field-lines. From now on, the curve  $\mathcal{C}$  that will be considered here is the magnetic axis, since we want to link the Floquet multipliers of  $\mathcal{C}$  to  $t_a$ . Variations of the axis geometry  $\delta\mathbf{x}$  are thus performed. Taking the variation of Eq.(3.2),

$$\delta^2 \mathcal{S}[\delta\mathbf{x}] = \oint_{\mathcal{C}} \delta(\mathbf{x}' \times \mathbf{B} \cdot \delta\mathbf{x}) d\ell = \oint_{\mathcal{C}} d\ell \delta\mathbf{x} \cdot (\delta\mathbf{x}' \times \mathbf{B} + \mathbf{x}' \times \delta\mathbf{B}), \quad (3.3)$$

where  $\mathbf{f}' := d\mathbf{f}/d\ell$  for any  $\mathbf{f}$ . Using  $\delta\mathbf{B} = \delta\mathbf{x} \cdot \nabla \mathbf{B}$  and the Einstein's summation convention, we write the second variation as an operator:

$$\begin{aligned} \delta^2 \mathcal{S} &= \oint_{\mathcal{C}} d\ell \delta\mathbf{x}^i \epsilon_{ijk} \left( \frac{d\delta\mathbf{x}^j}{d\ell} \mathbf{B}^k + \mathbf{x}'^j \delta\mathbf{x}^m \partial_m \mathbf{B}^k \right) \\ &= \oint_{\mathcal{C}} d\ell \delta\mathbf{x}^i \frac{\delta^2 S}{\delta\mathbf{x}^i \delta\mathbf{x}^j} \delta\mathbf{x}^j, \end{aligned} \quad (3.4)$$

where,

$$\frac{\delta^2 \mathcal{S}}{\delta\mathbf{x}^i \delta\mathbf{x}^j} = \epsilon_{ijk} \mathbf{B}^k \frac{d}{d\ell} + \epsilon_{imk} \mathbf{x}'^m \partial_j \mathbf{B}^k \quad (3.5)$$

which in matrix form, reads:

$$\overline{\overline{\mathcal{M}}} \equiv \frac{\delta^2 \mathcal{S}}{\delta\mathbf{x} \delta\mathbf{x}} = -(\mathbb{I} \times \mathbf{B}) \frac{d}{d\ell} + \mathbf{x}' \times (\nabla \mathbf{B})^\top. \quad (3.6)$$

Note that the covariant tensor  $\overline{\overline{\mathcal{M}}}$  can be easily symmetrized (see Hudson and Dewar (2009)). However, the direction in which the derivative  $d/d\ell$  is taken has to be chosen carefully. We shall continue with the non-symmetric form Eq.(3.6).

In what follows, we will show that the null eigenvalues and the eigenfunctions of  $\overline{\overline{\mathcal{M}}}$  are of particular interest in order to compute the Floquet exponents. Indeed, the eigenvalues and eigenfunctions of  $\overline{\overline{\mathcal{M}}}$  are related to the exponents and the normal form of the field-line Hamiltonian near the magnetic axis (see Duignan and Meiss (2021)). Let  $\mathbf{v}$  be a null eigenfunction of  $\overline{\overline{\mathcal{M}}}$  such that

$$\overline{\overline{\mathcal{M}}} \cdot \mathbf{v} = \mathbf{0}. \quad (3.7)$$

For  $\mathbf{v}$  to be nontrivial we must have

$$\det(\overline{\overline{\mathcal{M}}}) = 0. \quad (3.8)$$

### 3.3. Consistency verifications: Mercier coordinates

We will show that the condition Eq.(3.8) is satisfied by the Floquet exponents (see 1.1), which will be demonstrated to be related to the on-axis rotational transform. To do so, we shall use the near-axis formalism developed by Mercier (see Mercier et al. (1987)), Solovev and Shafranov (see Solovev and Shafranov (1970)), which utilizes the Frenet-Serret frame. As of the eigenvector interpretation, they correspond to the directions in which the axis is displaced, to keep nearby trajectories extremizing the action.

## 3.3 Consistency verifications: Mercier coordinates

Before introducing the theory of the infinite Hill's determinant (to solve Eq.(3.8)), we demonstrate that the second variation enables indeed to link the Floquet exponents to the rotational transform, by developing the second variation tensor equation Eq.(3.7) in Mercier coordinates.

### 3.3.1 The second variation of the action in Mercier coordinates

In what follows, the objective is to recover the on-axis rotational transform expression from Mercier Eq.(2). We use Mercier's coordinate system, which is based on the Frenet-Serret frame  $\{\mathbf{t}, \mathbf{n}, \mathbf{b}\}$  (see appendix A.5). The magnetic axis  $\mathbf{x}_0(\ell)$  forms a closed curve  $\mathcal{C}$  parametrized by the arclength  $\ell$  and a total length  $L$ . Following Mercier (Mercier et al. (1987)), we construct a tube of radius  $\rho$  around the axis, such that any point around the axis can be described by

$$\mathbf{x} = \mathbf{x}_0(\ell) + \rho \boldsymbol{\rho}, \quad \mathbf{x}'_0(\ell) = \mathbf{t}. \quad (3.9)$$

Here,  $\{\mathbf{t}, \boldsymbol{\rho}, \boldsymbol{\omega}\}$  is a right-handed triad related to the Frenet-Serret frame  $\{\mathbf{t}, \mathbf{n}, \mathbf{b}\}$  through a rotation by an angle  $\theta$  in the normal-binormal plane (see Fig.(3.1)), i.e.

$$\boldsymbol{\rho} = \mathbf{n} \cos \theta + \mathbf{b} \sin \theta, \quad \boldsymbol{\omega} = \mathbf{b} \cos \theta - \mathbf{n} \sin \theta. \quad (3.10)$$

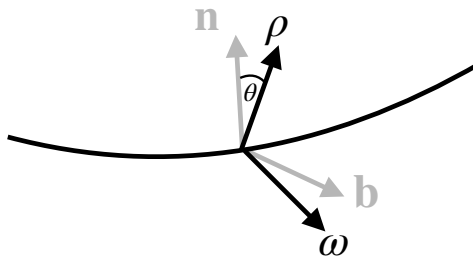


Figure 3.1 – Mercier coordinate system and how it is related to the Frenet-Serret system. The plain black line is a field line.

Mercier showed that  $(\rho, \omega = \theta + \int \tau d\ell, \ell)$ , with  $\tau$  the torsion, forms an orthogonal coordinate system with the metric

$$ds^2 = d\rho^2 + \rho^2 d\omega^2 + h^2 d\ell^2, \quad h = 1 - \kappa\rho \cos \theta, \quad (3.11)$$

where  $\kappa$  denotes the curvature (see appendix A.5). From now on, Mercier coordinates  $(\rho, \omega, \ell)$  will be used. Thus, let us introduce a few useful identities:

$$\begin{aligned} \mathbb{I} &= \boldsymbol{\rho}\boldsymbol{\rho} + \boldsymbol{\omega}\boldsymbol{\omega} + \mathbf{t}\mathbf{t}, \quad \nabla = \boldsymbol{\rho}\partial_\rho + \frac{\boldsymbol{\omega}}{\rho}\partial_\omega + \frac{\mathbf{t}}{h}\partial_\ell \\ \boldsymbol{\rho}_{,\omega} &= \boldsymbol{\omega}, \quad \boldsymbol{\rho}_{,\ell} = -\mathbf{t} \kappa \cos \theta, \quad \boldsymbol{\omega}_{,\omega} = -\boldsymbol{\rho}, \quad \boldsymbol{\omega}_{,\ell} = \mathbf{t} \kappa \sin \theta \\ \nabla \mathbf{t} &= \mathbf{t}\mathbf{n} \frac{\kappa}{h}, \quad \nabla \boldsymbol{\rho} = \boldsymbol{\omega}\boldsymbol{\omega} \frac{1}{\rho} - \mathbf{t}\mathbf{t} \frac{\kappa \cos \theta}{h}, \quad \nabla \boldsymbol{\omega} = -\boldsymbol{\omega}\boldsymbol{\rho} \frac{1}{\rho} + \mathbf{t}\mathbf{t} \frac{\kappa \sin \theta}{h} \end{aligned}$$

where the subscripted commas denote derivatives with respect to the argument on their right.

To determine the behavior near the magnetic axis, we carry out an expansion in the parameter  $\kappa\rho \ll 1$ . To evaluate  $\overline{\mathcal{M}}$  to lowest order in  $\kappa\rho$ , we need to expand the magnetic field up to first order. Therefore, we assume:

$$\mathbf{B} = B_0(\ell)\mathbf{t} + \rho\mathbf{B}_1, \quad \mathbf{B}_1 = \left( B_1^\rho \boldsymbol{\rho} + B_1^\omega \boldsymbol{\omega} + B_1^t \mathbf{t} \right). \quad (3.12)$$

Next, we calculate  $\nabla\mathbf{B}$ , which appears in  $\overline{\mathcal{M}}$ . From Eq.(3.12) and Eq.(3.12)

$$\nabla\mathbf{B} = \frac{1}{h} (\mathbf{t}\mathbf{t} B'_0(\ell) + \mathbf{t}\mathbf{n} \kappa B_0) + \boldsymbol{\rho} \mathbf{B}_1 + \rho \nabla\mathbf{B}_1. \quad (3.13)$$

To lowest order in  $\kappa\rho$ , the last term,  $\rho\nabla\mathbf{B}_1$ , after some algebra can be simplified to

$$\rho\nabla\mathbf{B}_1 = \boldsymbol{\omega}\boldsymbol{\omega} (\partial_\omega B_1^\omega + B_1^\rho) + \boldsymbol{\omega}\mathbf{t} \partial_\omega B_1^t + \boldsymbol{\omega}\boldsymbol{\rho} (\partial_\omega B_1^\rho - B_1^\omega), \quad (3.14)$$

such that, to leading order we have

$$\begin{aligned} \mathbf{x}' \times \nabla\mathbf{B}^\top &= \kappa B_0 \mathbf{b}\mathbf{t} + (B_1^\rho \boldsymbol{\omega} - B_1^\omega \boldsymbol{\rho}) \boldsymbol{\rho} + \boldsymbol{\omega}\boldsymbol{\omega} (\partial_\omega B_1^\rho - B_1^\omega) - \boldsymbol{\omega}\boldsymbol{\rho} (\partial_\omega B_1^\omega + B_1^\rho) \quad (3.15) \\ -(\mathbb{I} \times \mathbf{B}) &= (\boldsymbol{\rho}\boldsymbol{\omega} - \boldsymbol{\omega}\boldsymbol{\rho}) B_0 \end{aligned}$$

Finally,  $\overline{\mathcal{M}}$  as given by Eq.(3.6) simplifies to

$$\overline{\mathcal{M}} \equiv \overline{\mathcal{M}}_1 \frac{d}{d\ell} + \overline{\mathcal{M}}_2 \quad (3.16)$$

$$\overline{\mathcal{M}}_1 = (\boldsymbol{\rho}\boldsymbol{\omega} - \boldsymbol{\omega}\boldsymbol{\rho}) B_0, \quad (3.17)$$

$$\overline{\mathcal{M}}_2 = \kappa B_0 \mathbf{b}\mathbf{t} + (B_1^\rho \boldsymbol{\omega} - B_1^\omega \boldsymbol{\rho}) \boldsymbol{\rho} + \boldsymbol{\omega}\boldsymbol{\omega} (\partial_\omega B_1^\rho - B_1^\omega) - \boldsymbol{\omega}\boldsymbol{\rho} (\partial_\omega B_1^\omega + B_1^\rho). \quad (3.18)$$

### 3.3.2 Imposing constraints from MHD

The MHD conditions must be enforced for physical consistency, to recover  $\tau_a$ . The force-balance condition does not appear until higher order since  $\nabla p = 0$  near the axis. However, we still need to impose  $\nabla \cdot \mathbf{B} = 0$  and  $\mathbf{J} = \nabla \times \mathbf{B} = J_0(\ell)\mathbf{t}$ . We assume to be working in a unit system such that  $\mu_0 = 1$ . The divergence and curl of  $\mathbf{B}$  can be evaluated directly from the  $\nabla \mathbf{B}$  tensor, using dyadic algebra. From

$$\begin{aligned}\nabla \cdot \mathbf{B} &= \mathbb{I} : \nabla \mathbf{B} = B'_0 + 2B_1^\rho + \partial_\omega B_1^\omega \\ \nabla \times \mathbf{B} &= \mathbb{I} \times \nabla \mathbf{B} = \mathbf{t} (2B_1^\omega - \partial_\omega B_1^\rho) + (\boldsymbol{\omega} - \boldsymbol{\rho} \partial_\omega) (B_0 \kappa \cos \theta - B_1^t)\end{aligned}\quad (3.19)$$

we get the conditions

$$B_1^t = \kappa B_0 \cos \theta, \quad (\partial_\omega B_1^\rho - B_1^\omega) = B_1^\omega - J_0, \quad -(\partial_\omega B_1^\omega + B_1^\rho) = B'_0 + B_1^\rho. \quad (3.20)$$

Furthermore, it can be easily shown that

$$B_1^t = \kappa B_0 \cos \theta, \quad B_1^\rho = -\frac{1}{2}(B'_0 + \partial_\omega b_1), \quad B_1^\omega = \frac{1}{2}J_0 + b_1, \quad (3.21)$$

where,  $b_1$  satisfies the Laplace equation

$$(\partial_\omega^2 + 4)b_1 = 0. \quad (3.22)$$

Following Mercier et al. (1987), the solution of Eq.(3.22) can be expressed as

$$\begin{aligned}b_1 &= b_{c2}(\ell) \cos 2u + b_{s2}(\ell) \sin 2u, \quad u = \theta + \delta(\ell) = \omega - \int \tau d\ell + \delta(\ell) \\ \frac{b_{s2}}{B_0} &= \frac{\eta'}{2}, \quad \frac{b_{c2}}{B_0} = \tanh \eta(\ell) \left( \delta' - \tau + \frac{J_0/2}{B_0} \right)\end{aligned}\quad (3.23)$$

The functions  $\eta(\ell)$  and  $\delta(\ell)$  control respectively the eccentricity and the rotation - see Fig.(3.2) - of the elliptic flux-surfaces, given by the flux function

$$\psi = \rho^2 B_0 (\cosh \eta + \sinh \eta \sin 2u). \quad (3.24)$$

Using the constraints from MHD, we can write the components of  $\overline{\mathcal{M}}$  in terms of sines and cosines of  $u$  and the following functions of  $\ell$ :  $B_0, J_0, \eta, \delta, \kappa, \tau$ .

$$\begin{aligned}\overline{\mathcal{M}} &= (\boldsymbol{\rho} \boldsymbol{\omega} - \boldsymbol{\omega} \boldsymbol{\rho}) B_0 \frac{d}{d\ell} + \kappa B_0 \mathbf{b} \mathbf{t} \\ &+ B_0 \tanh(\eta) \left( \delta' - \tau + \frac{J_0}{2B_0} \right) \left\{ \cos(2u) [5\boldsymbol{\omega} \boldsymbol{\omega} + \boldsymbol{\rho} \boldsymbol{\rho}] + \sin(2u) [2\boldsymbol{\omega} \boldsymbol{\rho}] \right\} \\ &- \eta' \frac{B_0}{2} \left\{ \cos(2u) [2\boldsymbol{\omega} \boldsymbol{\rho}] + \sin(2u) [5\boldsymbol{\omega} \boldsymbol{\omega} + \boldsymbol{\rho} \boldsymbol{\rho}] \right\} - \frac{J_0}{2} [\boldsymbol{\omega} \boldsymbol{\omega} + \boldsymbol{\rho} \boldsymbol{\rho}].\end{aligned}\quad (3.25)$$

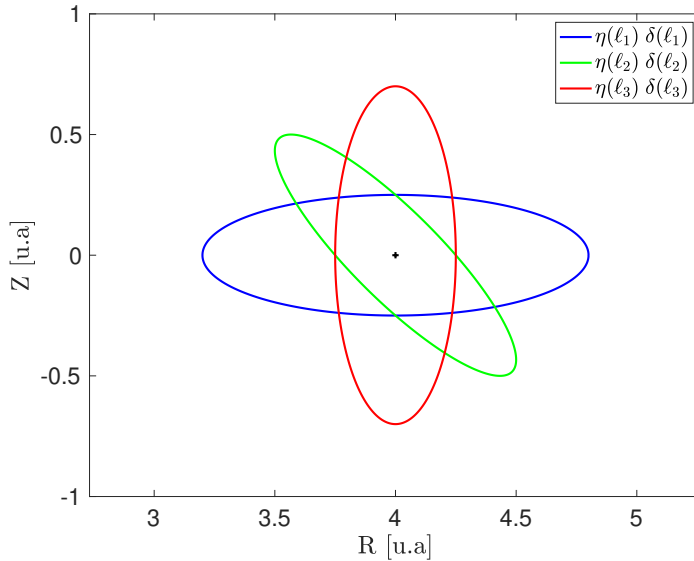


Figure 3.2 – Rotated elliptical cross sections centered around the magnetic axis with rotation parameter and eccentricity varying with  $\ell$ . This configuration does not represent a particular stellarator, but illustrates the parameters  $\eta$  and  $\delta$ .

### 3.3.3 Floquet exponents and rotational transform

Now that the MHD constraints have been enforced, let us obtain the null eigenvector  $\mathbf{v} = v^t \mathbf{t} + v^\rho \boldsymbol{\rho} + v^\omega \boldsymbol{\omega}$  of  $\overline{\mathcal{M}}$  such that  $\overline{\mathcal{M}} \cdot \mathbf{v} = 0$ , in order to determine the Floquet exponents. Let us take advantage of the fact that Mercier's coordinates are orthogonal (so the contravariant and covariant coordinates of vectors in that basis are equal), to avoid a heavy notation, with superscript for components *and* derivatives. However, when carrying on similar derivations, one has to be careful with the nature of the components they are working with. We state that the components  $v_t, v_\rho, v_\omega$  are functions of  $\omega$  and  $\ell$ .

The  $\overline{\overline{\mathcal{M}_1}}$  term can be shown to be

$$\overline{\overline{\mathcal{M}_1}} \frac{d}{d\ell} \cdot \mathbf{v} = B_0 \left( \boldsymbol{\rho} (v'_\omega - \kappa \sin \theta v_t) - \boldsymbol{\omega} (v'_\rho + \kappa \cos \theta v_t) \right) \quad (3.26)$$

Similarly,

$$\begin{aligned} \overline{\overline{\mathcal{M}_2}} \cdot \mathbf{v} &= \boldsymbol{\rho} (B_0 v'_\omega + v_\omega (B'_0 + B_{1\rho}) - B_{1\omega} v_\rho) \\ &\quad + \boldsymbol{\omega} (-B_0 v'_\rho + v_\omega (B_{1\omega} - J_0) + B_{1\rho} v_\rho) \end{aligned} \quad (3.27)$$

Thus, we observe that  $\overline{\overline{\mathcal{M}}} \cdot \mathbf{v} = 0$  only has  $\boldsymbol{\rho}, \boldsymbol{\omega}$  components with  $\ell$  derivatives of  $v_\rho, v_\omega$ . The tangential component  $v_t$  is thus an arbitrary constant, which can be absorbed by redefining  $v_\rho, v_\omega$ . We shall therefore set  $v_t = 0$ . This is consistent with the statement

### 3.3. Consistency verifications: Mercier coordinates

---

Eq.(3.15) that the projection of Eq.(3.7) along  $\mathbf{t}$  is trivial.

The condition  $\overline{\overline{\mathcal{M}}} \cdot \mathbf{v} = 0$  leads to the system

$$B_0 \begin{pmatrix} 0 & +1 \\ -1 & 0 \end{pmatrix} \frac{d}{d\ell} \begin{pmatrix} v_\rho \\ v_\omega \end{pmatrix} + \begin{pmatrix} -B_{1\omega} & (B'_0 + B_{1\rho}) \\ +B_{1\rho} & (B_{1\omega} - J_0) \end{pmatrix} \begin{pmatrix} v_\rho \\ v_\omega \end{pmatrix} = 0. \quad (3.28)$$

Substituting the MHD constraints into Eq.(3.28), we obtain the equivalent system of coupled linear PDEs:

$$\begin{cases} v'_\omega + \left( \frac{B'_0}{2B_0} - \frac{\partial_\omega b_1}{2B_0} \right) v_\omega - \left( \frac{J_0/2}{B_0} + \frac{b_1}{B_0} \right) v_\rho = 0 \\ v'_\rho + \left( \frac{B'_0}{2B_0} + \frac{\partial_\omega b_1}{2B_0} \right) v_\omega + \left( \frac{J_0/2}{B_0} - \frac{b_1}{B_0} \right) v_\omega = 0 \end{cases} \quad (3.29)$$

$$\begin{cases} v'_\omega + \left( \frac{B'_0}{2B_0} - \frac{\partial_\omega b_1}{2B_0} \right) v_\omega - \left( \frac{J_0/2}{B_0} + \frac{b_1}{B_0} \right) v_\rho = 0 \\ v'_\rho + \left( \frac{B'_0}{2B_0} + \frac{\partial_\omega b_1}{2B_0} \right) v_\omega + \left( \frac{J_0/2}{B_0} - \frac{b_1}{B_0} \right) v_\omega = 0 \end{cases} \quad (3.30)$$

Interpreting the  $\ell$  derivative along the first order field lines, both the forms Eq.(3.29-3.30) can be represented in the form

$$\frac{d\tilde{\mathbf{v}}}{d\ell} = A(\ell)\tilde{\mathbf{v}}, \quad \tilde{\mathbf{v}} = (v_\rho, v_\omega). \quad (3.31)$$

Here,  $A(\ell)$  is a matrix with components periodic in  $\ell$ . Note that this is always possible to do since along the field line  $\omega$  must be considered a function of  $\ell$  (see Solovev and Shafranov (1970), Duignan and Meiss (2021)). Such an approach will be useful to evaluate the determinant of  $\overline{\overline{\mathcal{M}}}$ , later on. We can directly use the Floquet-Lyapunov theorem on Eq.(3.31) to conclude that the solution must be of the form

$$\tilde{\mathbf{v}} = U(\ell)e^{C\ell/L}, \quad (3.32)$$

where  $U$  is a symplectic periodic matrix and  $C$  is a constant Hamiltonian matrix. The eigenvalues of  $C$  are the Floquet multipliers, which must be of the form  $e^{\pm i\nu}$  ( $\nu \in \mathbb{R}$ ) near an elliptic axis.

An equivalent approach is to solve the system from Eq.(3.29) using the fact that  $b_1$  only has second harmonics in  $u$ . This allows us to seek for a solution, where  $\tilde{\mathbf{v}}$  has only first harmonics in  $u$ . From now on, we will follow this approach. We'll show that there exists a solution to  $\overline{\overline{\mathcal{M}}} \cdot \mathbf{v} = 0$  with

$$\begin{pmatrix} v_\rho(\ell) \\ v_\omega(\ell) \end{pmatrix} = \begin{pmatrix} v_{\rho c}(\ell) \\ v_{\omega c}(\ell) \end{pmatrix} \cos u + \begin{pmatrix} v_{\rho s}(\ell) \\ v_{\omega s}(\ell) \end{pmatrix} \sin u, \quad u = \omega - \int \tau d\ell + \delta(\ell). \quad (3.33)$$

Substituting the above together with the expressions for  $B_{1\rho}, B_{1\omega}$  from Eq.(3.21) into Eq.(3.29), yields first and third harmonics of  $u$ . Equating the  $\sin u, \cos u$  terms, the  $v'_\omega$  equation yields

$$\begin{cases} v'_{\omega c} - (\tau - \delta') v_{\omega s} - \left( \frac{J_0/2}{B_0} \right) v_{\rho c} + \frac{B'_0}{2B_0} v_{\omega c} + \frac{1}{2} (\alpha_{c2c} + \alpha_{s2s}) = 0 \\ v'_{\omega s} + (\tau - \delta') v_{\omega c} - \left( \frac{J_0/2}{B_0} \right) v_{\rho s} + \frac{B'_0}{2B_0} v_{\omega s} + \frac{1}{2} (\alpha_{s2c} - \alpha_{c2s}) = 0 \end{cases} \quad (3.34)$$

Equating the third harmonics lead to the following constraints

$$\alpha_{c2c} = \alpha_{s2s}, \quad \alpha_{s2c} = -\alpha_{c2s}, \quad (3.35)$$

where,  $\alpha'$ s have the following definitions

$$\begin{aligned} \alpha_{c2c} &= -\frac{b_{c2}}{B_0} v_{\rho c} - \frac{b_{s2}}{B_0} v_{\omega c}, & \alpha_{s2s} &= -\frac{b_{s2}}{B_0} v_{\rho s} + \frac{b_{c2}}{B_0} v_{\omega s} \\ \alpha_{s2c} &= -\frac{b_{s2}}{B_0} v_{\rho c} + \frac{b_{c2}}{B_0} v_{\omega c}, & \alpha_{c2s} &= -\frac{b_{c2}}{B_0} v_{\rho s} - \frac{b_{s2}}{B_0} v_{\omega s} \end{aligned} \quad (3.36)$$

The constraint Eq.(3.35) and the definitions from Eq.(3.36) imply

$$\begin{pmatrix} b_{s2} & b_{c2} \\ -b_{c2} & b_{s2} \end{pmatrix} \begin{pmatrix} v_{\omega c} - v_{\rho s} \\ v_{\omega s} + v_{\rho c} \end{pmatrix} = 0 \quad (3.37)$$

Since the determinant  $b_{s2}^2 + b_{c2}^2 \neq 0$  we must have

$$v_{\rho s} = v_{\omega c}, \quad v_{\rho c} = -v_{\omega s}, \quad (3.38)$$

which allows us to rewrite Eq.(3.34) solely in terms of  $v_{\omega c}, v_{\omega s}$ . Simplification leads to

$$\begin{cases} v'_{\omega c} + \left( \frac{B'_0}{2B_0} - \frac{b_{s2}}{B_0} \right) v_{\omega c} + \left( \frac{J_0/2}{B_0} - \tau + \delta' + \frac{b_{c2}}{B_0} \right) v_{\omega s} = 0 \\ v'_{\omega s} + \left( \frac{B'_0}{2B_0} + \frac{b_{s2}}{B_0} \right) v_{\omega s} - \left( \frac{J_0/2}{B_0} - \tau + \delta' - \frac{b_{c2}}{B_0} \right) v_{\omega c} = 0. \end{cases} \quad (3.39)$$

Finally, using the MHD constraints Eq.(3.23), we get

$$\begin{cases} v'_{\omega c} + \left( \frac{B'_0}{2B_0} - \frac{\eta'}{2} \right) v_{\omega c} + \frac{e^{+\eta}}{\cosh(\eta)} \left( \frac{J_0/2}{B_0} - \tau + \delta' \right) v_{\omega s} = 0 \\ v'_{\omega s} + \left( \frac{B'_0}{2B_0} + \frac{\eta'}{2} \right) v_{\omega s} - \frac{e^{-\eta}}{\cosh(\eta)} \left( \frac{J_0/2}{B_0} - \tau + \delta' \right) v_{\omega c} = 0. \end{cases} \quad (3.40)$$

### 3.3. Consistency verifications: Mercier coordinates

---

Although Eq.(3.40) is already in a form from which the Floquet exponents can be calculated, it is possible to further simplify the system by introducing new variables  $(X, Y)$ ,

$$v_{\omega c} = \frac{1}{\sqrt{B'_0}} e^{+\eta/2} X(\ell), \quad v_{\omega s} = \frac{1}{\sqrt{B'_0}} e^{-\eta/2} Y(\ell) \quad (3.41)$$

such that Eq.(3.40) reduces to

$$X' + \Omega_0(\ell)Y = 0, \quad Y' - \Omega_0(\ell)X = 0, \quad \Omega_0(\ell) = \frac{\frac{J_0/2}{B'_0} - \tau + \delta'}{2 \cosh \eta} \quad (3.42)$$

The Eq.(3.42) is a simple harmonic oscillator system with a 'time'-dependent frequency. Using the complex variable  $Z = X + iY$  we can rewrite as a single complex ODE

$$Z' - i\Omega_0 Z = 0 \quad \Rightarrow \quad Z(\ell) = Z_0 \exp \int_0^\ell i\Omega_0(s) ds \quad (3.43)$$

Separating the periodic and non-periodic parts of the exponential we get

$$\begin{aligned} Z(\ell) &= Z_p(\ell) e^{i\nu\ell/L}, \quad Z_p(\ell) = Z_0 \exp \int_0^\ell i\tilde{\Omega}_0(s) ds, \\ \bar{\Omega} &\equiv \frac{1}{L} \int_0^L \Omega_0(s) ds, \quad \tilde{\Omega}_0 = \Omega_0(\ell) - \bar{\Omega}. \end{aligned} \quad (3.44)$$

Comparing Eq.(3.44) with Eq.(3.32), we find that  $\nu$ , given by

$$\nu = \int_0^L \Omega_0(s) ds = \oint \frac{\frac{J_0(s)/2}{B_0(s)} - \tau(s) + \delta'(s)}{2 \cosh \eta(s)} ds, \quad (3.45)$$

is the Floquet exponent for the system. Furthermore, this matches the expression for the rotational transform derived by Mercier. Therefore it follows that the null eigenvalue of the second variation tensor yields the correct on-axis rotational transform. The contribution that is aimed to be brought by mean of this method is to later apply it to some more general curves, where the Mercier formula cannot be applied, such as in the neighborhood of X-points.

### 3.4 Floquet exponents from infinite Hill's determinant

Now that the second variation tensor has been proven to enable to compute  $\tau_a$ , let us introduce a more general system of coordinates, in which expanding the second variation yields the theory of the infinite Hill's determinant, enabling to compute the Floquet exponents. The Solovev-Shafranov coordinates are closely related to the Mercier ones, and use as a starting point the Frenet-Serret frame too.

#### 3.4.1 The second variation of the action in Solovev-Shafranov coordinates

Let  $(\mathbf{t}, \mathcal{N}, \mathcal{B})$  be the orthogonal triad related to the Frenet Serret frame through a rotation by angle  $\delta$  such that

$$\mathcal{N} = \mathbf{n} \cos \delta - \mathbf{b} \sin \delta, \quad \mathcal{B} = \mathbf{n} \sin \delta + \mathbf{b} \cos \delta. \quad (3.46)$$

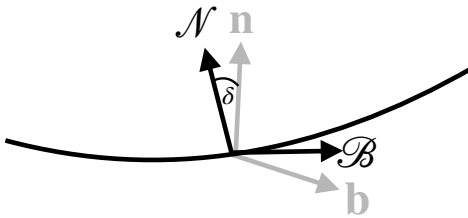


Figure 3.3 – Solovev-Shafranov coordinate system and how it is related to the Frenet-Serret system. As in Fig.(3.1), the plain black line is a field line.

In terms of the Mercier angle  $u$  and the unit vectors  $(\boldsymbol{\rho}, \boldsymbol{\omega})$ , we can represent  $(\mathcal{N}, \mathcal{B})$  as

$$\mathcal{N} = \boldsymbol{\rho} \cos u - \boldsymbol{\omega} \sin u, \quad \mathcal{B} = \boldsymbol{\rho} \sin u + \boldsymbol{\omega} \cos u \quad (3.47)$$

It follows from the Frenet-Serret equations and (3.46) that

$$\mathcal{N}' = -\kappa \cos \delta \mathbf{t} - u' \mathcal{N} - \mathcal{B}, \quad \mathcal{B}' = -\kappa \sin \delta \mathbf{t} + u' \mathcal{N}, \quad u'(\ell) = \delta'(\ell) - \tau(\ell). \quad (3.48)$$

Following Solovev and Shafranov (1970), the position vector  $\mathbf{r}$  of any point can be expressed as

$$\mathbf{r} = \mathbf{r}_0 + x \mathcal{N} + y \mathcal{B}, \quad (3.49)$$

which rewrites, in terms of Mercier coordinates

$$x = \rho \cos u, \quad y = \rho \sin u. \quad (3.50)$$

### 3.4. Floquet exponents from infinite Hill's determinant

---

Differentiating (3.49) with respect to  $\ell$ , we get

$$\frac{d\mathbf{r}}{d\ell} = h\mathbf{t} + \mathcal{N}(x' + u'y) + \mathcal{B}(y' - u'x). \quad (3.51)$$

Therefore, multiplying by  $d\ell$ , the metric obtained from (3.51) reads

$$ds^2 = dx^2 + dy^2 + 2u'd\ell(ydx - xdy) + d\ell^2(h^2 + u'^2(x^2 + y^2)), \quad (3.52)$$

with the following metric tensor in contravariant and covariant forms respectively:

$$\begin{aligned} g_{ij} &= \begin{pmatrix} 1 & 0 & u'y \\ 0 & 1 & -u'x \\ u'y & -u'x & h^2 + u'^2(x^2 + y^2) \end{pmatrix}, \\ g^{ij} &= \frac{1}{h^2} \begin{pmatrix} h^2 + u'^2y^2 & -u'^2xy & -u'y \\ -u'^2xy & 1 & u'x \\ -u'y & u'x & 1 \end{pmatrix}, \quad \sqrt{g} = h. \end{aligned} \quad (3.53)$$

It can be seen by direct substitution that the following basis vectors lead to the same metric tensor as (3.53):

$$\mathbf{e}^1 = \nabla x = \mathcal{N} - \frac{u'y}{h}\mathbf{t}, \quad \mathbf{e}^2 = \nabla y = \mathcal{B} + \frac{u'x}{h}\mathbf{t}, \quad \mathbf{e}^3 = \nabla \ell = \frac{1}{h}\mathbf{t} \quad (3.54)$$

and

$$\begin{aligned} \mathbf{e}_1 &= h\nabla y \times \nabla \ell = \mathcal{N}, \quad \mathbf{e}_2 = h\nabla \ell \times \nabla x = \mathcal{B}, \\ \mathbf{e}_3 &= h\nabla x \times \nabla y = ht + u'(-x\mathcal{B} + y\mathcal{N}). \end{aligned} \quad (3.55)$$

#### Magnetic field near a closed field line

So far everything is exact. To compute the second variation of  $\mathcal{S}$ , we shall now expand the field in small  $x, y$ , restricting ourselves only to linear terms (or equivalently, first-order in  $\rho$ ). In this approximation, the magnetic field can be written in contravariant form as

$$\sqrt{g}\mathbf{B} = \sqrt{g}B^1\mathbf{e}_1 + \sqrt{g}B^2\mathbf{e}_2 + \sqrt{g}B^3\mathbf{e}_3, \quad (3.56)$$

and each component is expressed as

$$\sqrt{g}B^1 = a_1x + a_2y, \quad \sqrt{g}B^2 = b_1x + b_2y, \quad \sqrt{g}B^3 = B_0 + c_1x + c_2y, \quad (3.57)$$

where,  $a_1, a_2, b_1, b_2$  are periodic functions of  $\ell$ . From (3.55) it then follows that

$$\mathbf{B} \approx (a_1 x + (a_2 + u' B_0) y) \mathcal{N} + ((b_1 - u' B_0) x + b_2 y) \mathcal{B} + (B_0 + c_1 x + c_2 y) \mathbf{t} \quad (3.58)$$

A direct calculation shows that, to lowest order,

$$\begin{aligned} \nabla \mathbf{B} &= \kappa B_0 \mathbf{t} \mathbf{n} + a_1 \mathcal{N} \mathcal{N} + b_2 \mathcal{B} \mathcal{B} + B'_0 \mathbf{t} \mathbf{t} + (a_2 + u' B_0) \mathcal{B} \mathcal{N} \\ &\quad + (b_1 - u' B_0) \mathcal{N} \mathcal{B} + (c_1 \mathcal{N} + c_2 \mathcal{B}) \mathbf{t} \\ \mathbf{x}' \times (\nabla \mathbf{B})^\top &= \kappa B_0 \mathbf{t} \mathbf{t} + \mathcal{B} (a_1 \mathcal{N} + (a_2 + u' B_0) \mathcal{B}) - \mathcal{N} ((b_1 - u' B_0) \mathcal{N} + b_2 \mathcal{B}), \end{aligned} \quad (3.59)$$

which yields, using dyadic algebra

$$\begin{aligned} \nabla \cdot \mathbf{B} &= \mathbb{I} : \nabla \mathbf{B} = B'_0 + a_1 + b_2 \\ \nabla \times \mathbf{B} &= -\mathbb{I} \times \nabla \mathbf{B} = \mathbf{t} (b_1 - a_2 - 2u' B_0) + \mathcal{N} (-\kappa B_0 \sin \delta + c_2) \\ &\quad - \mathcal{B} (c_1 - \kappa B_0 \cos \delta). \end{aligned} \quad (3.60)$$

Here we have used Eq.(3.46) to rewrite  $\mathbf{b}$  in terms of  $\mathcal{N}, \mathcal{B}$ . Therefore, imposing that  $\nabla \cdot \mathbf{B} = 0$  and  $\nabla \times \mathbf{B} = J_0 \mathbf{t}$ , we find

$$a_1 + b_2 = -B'_0, \quad \frac{b_1 - a_2}{2B_0} = u' + \frac{J_0/2}{B_0}, \quad c_1 = \kappa B_0 \cos \delta, \quad c_2 = \kappa B_0 \sin \delta \quad (3.61)$$

So far we only have two constraints for the four quantities  $a_1, a_2, b_1, b_2$ . Therefore, we need two more conditions to fully determine them. Hence we turn to the Mercier representation Eq.(3.23) of  $\mathbf{B}$ . Using Eq.(3.47) and basic trigonometry identities we obtain

$$\begin{aligned} \frac{\mathbf{B}}{B_0} &= \mathbf{t} (1 + \kappa \rho \cos \theta) + \mathcal{N} \left( -\frac{1}{2} \left( \frac{B'_0}{B_0} + \eta' \right) x + \left( \frac{-J_0}{2B_0} + \Omega_0 \sinh \eta \right) y \right) \\ &\quad + \mathcal{B} \left( \left( \frac{J_0}{2B_0} + \Omega_0 \sinh \eta \right) x - \frac{1}{2} \left( \frac{B'_0}{B_0} - \eta' \right) y \right). \end{aligned} \quad (3.62)$$

Comparing the Mercier representation Eq.(3.62) with the Solovev-Shafranov representation Eq.(3.58), we obtain for the expansion coefficients

$$\begin{aligned} \frac{a_1}{B_0} &= -\frac{1}{2} \left( \frac{B'_0}{B_0} + \eta' \right), \quad \frac{a_2}{B_0} = -\left( u' + \frac{J_0/2}{B_0} \right) + \Omega_0 \sinh \eta, \\ \frac{b_2}{B_0} &= -\frac{1}{2} \left( \frac{B'_0}{B_0} - \eta' \right), \quad \frac{b_1}{B_0} = \left( u' + \frac{J_0/2}{B_0} \right) + \Omega_0 \sinh \eta, \end{aligned} \quad (3.63)$$

which clearly satisfy Eq.(3.61).

### 3.4. Floquet exponents from infinite Hill's determinant

---

From the definition of  $\Omega_0$  Eq.(3.42) we can further simplify  $a_2, b_1$  as

$$\frac{a_2}{B_0} = -\Omega_0 e^{-\eta}, \quad \frac{b_1}{B_0} = \Omega_0 e^\eta \quad (3.64)$$

As a check of the correctness of the above expressions, we can show that  $\mathbf{B} \cdot \nabla \psi = 0$ , where

$$\begin{aligned} \sqrt{g} \mathbf{B} \cdot \nabla &= \sqrt{g} B^1 \partial_x + \sqrt{g} B^2 \partial_y + \sqrt{g} B^3 \partial_\ell \\ &= B_0 \partial_\ell + (a_1 x + a_2 y) \partial_x + (b_1 x + b_2 y) \partial_y \end{aligned} \quad (3.65)$$

The flux surface label  $\psi$  is given in the Mercier representation by Eq.(3.24) or equivalently in the Solovev-Shafranov representation as

$$\psi = B_0(e^\eta x^2 + e^{-\eta} y^2). \quad (3.66)$$

#### The second variation tensor

Now that the magnetic field has been properly expressed and expanded for nearby field lines in Solovev-Shafranov coordinates, we can substitute the obtained  $\mathbf{B}$  and  $\nabla \mathbf{B}$  in Eq.(3.6) and expand the second variation tensor. From Eq.(3.59) we find that it is given by

$$\overline{\mathcal{M}} \equiv \overline{\mathcal{M}_1} \frac{d}{d\ell} + \overline{\mathcal{M}_2} \quad (3.67)$$

$$\overline{\mathcal{M}_1} = (\mathcal{N} \mathbf{B} - \mathbf{B} \mathcal{N}) B_0, \quad (3.68)$$

$$\overline{\mathcal{M}_2} = \kappa B_0 \mathbf{b} \mathbf{t} + \mathbf{B} (a_1 \mathcal{N} + (a_2 + u' B_0) \mathbf{B}) - \mathcal{N} ((b_1 - u' B_0) \mathcal{N} + b_2 \mathbf{B}). \quad (3.69)$$

As in the Mercier expansion case, we choose the null eigenvector  $\mathbf{v} = v_N \mathcal{N} + v_B \mathbf{B}$  of  $\overline{\mathcal{M}}$  such that  $\overline{\mathcal{M}} \cdot \mathbf{v} = 0$ . We note that

$$\frac{d}{d\ell} \mathbf{v} = (v'_N + u' v_B) \mathcal{N} + (v'_B - u' v_N) \mathbf{B} + (\dots) \mathbf{t} \quad (3.70)$$

The tangential terms  $\propto \mathbf{t}$  are not relevant since they do not contribute to  $\overline{\mathcal{M}} \cdot \mathbf{v} = 0$  because of the forms Eq.(3.68)-(3.69). The equations for  $(v_N, v_B)$  then read

$$B_0 \begin{pmatrix} 0 & +1 \\ -1 & 0 \end{pmatrix} \frac{d}{d\ell} \begin{pmatrix} v_N \\ v_B \end{pmatrix} + \begin{pmatrix} -b_1/B_0 & -b_2/B_0 \\ a_1/B_0 & a_2/B_0 \end{pmatrix} \begin{pmatrix} v_N \\ v_B \end{pmatrix} = 0. \quad (3.71)$$

Alternatively, we can rewrite Eq.(3.71) in the following ODE form

$$\frac{dv_B}{a_1 v_N + a_2 v_B} = \frac{dv_B}{b_1 v_N + b_2 v_B} = \frac{d\ell}{B_0}. \quad (3.72)$$

It is clear from Eq.(3.72) that the eigenvector  $\mathbf{v}$  satisfies the general characteristic equation for the expansion parameters  $(\mathcal{X}, \mathcal{Y})$ , along the magnetic field:

$$\frac{d\mathcal{X}}{\sqrt{g}B^1(\mathcal{X}, \mathcal{Y}, \ell)} = \frac{d\mathcal{Y}}{\sqrt{g}B^2(\mathcal{X}, \mathcal{Y}, \ell)} = \frac{d\ell}{\sqrt{g}B^3(\mathcal{X}, \mathcal{Y}, \ell)} \quad (3.73)$$

Thus, we can identify  $v_N, v_B$  with  $\mathcal{X}, \mathcal{Y}$ , the displacements of the magnetic field line from the closed field line  $\mathbf{B}_0$  along the normal and the binormal direction. We distinguish between  $(x, y)$ , which are coordinates and  $(\mathcal{X}, \mathcal{Y})$ , which are the solutions of the ODEs Eq.(3.73).

Written out explicitly, the equations for  $(\mathcal{X}, \mathcal{Y})$  are

$$\begin{aligned} \mathcal{X}' + \frac{1}{2} \left( \frac{B'_0}{B_0} + \eta' \right) \mathcal{X} + \Omega_0 e^{-\eta} \mathcal{Y} &= 0 \\ \mathcal{Y}' + \frac{1}{2} \left( \frac{B'_0}{B_0} - \eta' \right) \mathcal{Y} - \Omega_0 e^{\eta} \mathcal{X} &= 0, \end{aligned} \quad (3.74)$$

Introducing the variables

$$\mathcal{X} = \frac{1}{\sqrt{B'_0}} e^{+\eta/2} X(\ell), \quad \mathcal{Y} = \frac{1}{\sqrt{B'_0}} e^{-\eta/2} Y(\ell) \quad (3.75)$$

Eq.(3.74) reduces to Eq.(3.42) as before. The Floquet exponent then follows from the integrated  $\Omega_0$  along the field line, which is a second confirmation that  $\delta^2 \mathcal{S}$  yields  $\omega_a$ .

### 3.4.2 Floquet exponents and the Hill's determinant

Here we shall pursue an alternative approach to obtaining the Floquet exponent using the theory of Hills infinite determinant (Magnus (1953)). We start with the system Eq.(3.74) written as

$$\mathcal{X}' = \frac{1}{B_0} (a_1 \mathcal{X} + a_2 \mathcal{Y}), \quad \mathcal{Y}' = \frac{1}{B_0} (b_1 \mathcal{X} + b_2 \mathcal{Y}) \quad (3.76)$$

Eliminating  $\mathcal{Y}$  from (3.76) we obtain the following second order ODE for  $\mathcal{X}$

$$\mathcal{X}'' + 2C_1 \mathcal{X} + C_2 = 0 \quad (3.77)$$

where,

$$2C_1 = -\frac{a'_2}{a_2} + 2\frac{B'_0}{B_0}, \quad C_2 = \mathcal{D} - \frac{a_2}{B_0} \left( \frac{a_1}{a_2} \right)', \quad \mathcal{D} = \frac{1}{B_0^2} (a_1 b_2 - a_2 b_1). \quad (3.78)$$

### 3.4. Floquet exponents from infinite Hill's determinant

---

We can eliminate the first derivative term from (3.77) by the change of variables

$$\mathcal{X} = \exp\left(-\int C_1 d\ell\right) \Psi = \frac{\sqrt{a_2}}{B_0} X \quad (3.79)$$

which leads to

$$\Psi'' + \omega^2 \Psi = 0, \quad \omega^2 \equiv C_2 - C'_1 - C_1^2. \quad (3.80)$$

Eq.(3.80) is in the form of Hill's equation or a Schrodinger equation with a periodic potential  $\omega$ . Before we proceed further, we note that the linear transformation (3.79) implies that both  $x$  and  $X$  have the same Floquet exponent. This is because the multiplication factor  $\sqrt{a_2}/B_0$  is periodic in nature and therefore does not change the Floquet exponent, which is a secular term.

Leveraging the periodicity of  $\omega^2$ ,  $\omega^2(\ell + L) = \omega^2(\ell)$ , we can Fourier expand it as follows

$$\omega^2(\ell) = \omega_0^2 + \sum_{k=1}^{\infty} \omega_0 \omega_k \exp\left(ik \frac{2\pi\ell}{L}\right) \quad (3.81)$$

Let the fundamental solutions of (3.80) be given by  $\Psi_{\pm}(\ell)$  such that

$$\Psi_+(0) = 1, \quad \Psi_-(0) = 0, \quad \Psi'_+(0) = 0, \quad \Psi'_-(0) = 1 \quad (3.82)$$

The Floquet solutions are given by

$$\Psi_+(\ell) = \exp(+i\nu\ell)\sigma_+(\ell), \quad \sigma_+(\ell + L) = \sigma_+(\ell), \quad \sigma_+(0) = 1, \quad (3.83)$$

$$\Psi_-(\ell) = \exp(-i\nu\ell)\sigma_-(\ell), \quad \sigma_-(\ell + L) = \sigma_-(\ell), \quad \sigma_-(0) = 0 \quad (3.84)$$

Differentiating  $\Psi_+(\ell)$  we get

$$\Psi'_+(\ell) = i\nu\Psi_+(\ell) + \exp(+i\nu\ell)\sigma'_+(\ell), \quad \sigma'_+(0) = -i\nu. \quad (3.85)$$

From (3.85) and (3.82) it then follows that

$$\Psi_+(L) = \exp(+i\nu L), \quad \Psi'_+(L) = 0 \quad (3.86)$$

Similarly it can be shown that

$$\Psi_-(L) = 0, \quad \Psi'_-(L) = \exp(-i\nu L) \quad (3.87)$$

Thus,

$$\Psi_+(L) + \Psi'_-(L) = 2 \cos \nu L. \quad (3.88)$$

Let us now Fourier expand the Floquet solution as

$$\begin{aligned}\Psi_+ &= e^{i\nu\ell} \sum_n b_n e^{i\frac{2\pi n}{L}\ell} \\ \Psi'_+ &= i\nu\Psi_+ + i\frac{2\pi n}{L} e^{i\nu\ell} \sum_n b_n e^{i\frac{2\pi n}{L}\ell} \\ \Psi''_+ &= \sum_n b_n \left( \nu + \frac{2\pi n}{L} \right)^2 e^{i\ell(\nu + \frac{2\pi n}{L})}\end{aligned}\tag{3.89}$$

To fully Fourier expand Eq.(3.80), we need the second term  $\omega^2\Psi_+$ :

$$\omega^2(\ell) = \sum_{k=0}^{\infty} \omega_0 \omega_k e^{i\frac{2\pi}{L}k\ell} \implies \omega^2\Psi_+ = \sum_{n>k} \omega_0 \omega_k b_n e^{i\ell(\nu + \frac{2\pi}{L}(n+k))}.\tag{3.90}$$

Therefore,

$$\begin{aligned}\left( \partial_\ell^2 + \omega^2 \right) \Psi_+ &= \sum_n e^{i\ell(\nu + \frac{2\pi}{L}n)} \left( b_n \left( \omega_0^2 - \left( \nu + \frac{2\pi n}{L} \right)^2 \right) + \sum_{n \neq k} b_{n-k} \omega_0 \omega_k \right) \\ &= \sum_n e^{i\ell(\nu + \frac{2\pi}{L}n)} \sum_m \tilde{B}_{nm} b_m,\end{aligned}\tag{3.91}$$

where

$$\tilde{B}_{nm} := \delta_{nm} \left( \omega_0^2 - \left( \nu + \frac{2\pi n}{L} \right)^2 \right) + \omega_0 \omega_n\tag{3.92}$$

Thus, the equation to determine the Floquet exponents  $\nu$  is

$$\sum_m \tilde{B}_{mn} b_m = 0\tag{3.93}$$

which yields the following determinant equation

$$\det(|B_{nm}|) = 0.\tag{3.94}$$

Moreover, the above determinant can be rewritten in the following way

$$\begin{aligned}\det|B_{nm}| &= \left( \omega_0^2 - \left( \nu + \frac{2\pi n}{L} \right)^2 \right) \Delta(\nu), \\ \Delta(\nu) &\equiv \det \left| \delta_{nm} + \frac{\omega_0 \omega_n}{\omega_0^2 - \left( \nu + \frac{2\pi n}{L} \right)^2} \right|,\end{aligned}\tag{3.95}$$

and then

$$\Delta(0) = \det \left| \delta_{nm} + \frac{\omega_0 \omega_n}{\omega_0^2 - \left( \frac{2\pi n}{L} \right)^2} \right|.\tag{3.96}$$

### 3.4. Floquet exponents from infinite Hill's determinant

---

For Eq.(3.94) to be verified, we need  $\Delta(\nu) = 0$ . Following Z. X. Wang (1989) we are now going to show that the exponents can be deduced from a simple expression. One notes that  $\Delta(\nu)$  is a  $2\pi$  periodic function, with poles in  $\nu = \pm\omega_0 - 2\pi n/L$ . It can be shown that the determinant is absolutely convergent in the whole  $\nu$ -plane, except for these poles. Therefore,  $\Delta$  is meromorphic. Moreover, when  $\mathcal{I}(\nu) \rightarrow \pm\infty$ ,  $\Delta(\nu) \rightarrow 1$ . Let us now define the complex function  $f$  as

$$f(\nu) \equiv \cot \frac{L}{2}(\nu - \sqrt{\omega_0}) - \cot \frac{L}{2}(\nu + \sqrt{\omega_0}). \quad (3.97)$$

It is useful to introduce  $f$  since it has the same poles as  $\Delta$  and has the same periodicity. Moreover, it is bounded as  $\mathcal{I}(\nu) \rightarrow \pm\infty$ . This way, there has to exist a constant  $K$  such that

$$D(\nu) \equiv \Delta(\nu) + Kf(\nu) \quad (3.98)$$

has no singularity in the whole  $\nu$  plane. Together with the fact that it is bounded as  $|\nu| \rightarrow \infty$ , according to Liouville's theorem,  $D$  is a constant function. In the limit  $|\nu| \rightarrow \infty$ , we see that  $D = 1$ . To determine  $K$ , take  $\nu = 0$ :

$$\nu = 0 \implies K = \frac{\Delta(0) - 1}{f(0)} = \frac{1 - \Delta(0)}{2 \cot \frac{\omega_0 L}{2}}. \quad (3.99)$$

Using the value of  $K$  from Eq.(3.99), the condition  $\Delta(\nu) = 0$  is equivalent to

$$\begin{aligned} 1 + \frac{1 - \Delta(0)}{2 \cot \frac{\omega_0 L}{2}} f(\nu) &= 0 \\ \implies \frac{1}{\sin^2 \frac{\omega_0 L}{2}} &= \frac{2}{L} \frac{(\Delta(0) - 1)}{\sin(\nu - \omega_0) \sin(\nu + \omega_0)} \end{aligned} \quad (3.100)$$

Therefore, the Floquet exponent equation reduces to

$$\sin^2 \nu \frac{L}{2} = \Delta(0) \sin^2 \frac{\omega_0 L}{2}. \quad (3.101)$$

Although Eq.(3.101) is very simple, one obstacle remains to compute the exponents: one has to evaluate the infinite determinant  $\Delta(0)$ . We refer to Z. X. Wang (1989) for some approximations of  $\Delta(0)$ . For instance, when the  $\omega_n$  are sufficiently small,  $\Delta(0)$  can be approximated by the order-3 determinant with  $B_{00}$  as central element (we remind that the determinant involves sums over all  $\mathbb{Z}$ ), providing

$$\Delta(0) \simeq 1 + \frac{2\omega_1^2}{\omega_0 (4 - \omega_0)^2} + \frac{2\omega_1^2 \omega_2}{\omega_0 (4 - \omega_0)^2} - \frac{\omega_2^2}{(4 - \omega_0)^2}. \quad (3.102)$$

However, this approximation breaks down when the coefficients become too important as  $n$  increases. As of the exponents computed, they might all not be suitable for  $\epsilon_a$ . One has to discard the results that are not relevant. Moreover, we emphasize that the exponents might be shifted by  $2k\pi/L$ , with  $k$  integer, without changing the mathematics

of the system by periodicity. However, one has to carefully choose the adapted value for  $t_a$ . This method needs to be tested computationally but this is beyond the scope of this thesis and will be the object of a future work. Nonetheless, one has to bear in mind that this method is based on the approximative evaluation of an infinite determinant to determine the rotational transform.

### 3.4.3 Summary

The infinite determinant was derived from the second variation of  $\mathcal{S}$  in Solovev-Shafranov coordinates. It has been shown in section 3.4 that upon using appropriate coordinates and substitutions, the correct expression for the on-axis rotational transform was recovered. The same kind of derivation has been carried on in Mercier coordinates, to support the result that variational calculus combined with Floquet theory and applied to the action  $\mathcal{S}$  yields the on-axis rotational transform. Stellarator design needs fast and accurate computation of  $t_a$  since the latter is an important parameter. Currently, the most widely used method to compute  $t_a$  is to use field-line tracing (TODOROKI (2003)). However, although very accurate, field-line tracing methods compute  $t$  as an infinite time limit as the computer goes along the line. Determining a stop condition for field-line tracing methods brings some arbitrariness and the idea of an infinite-time limit is not pleasing. In the following section, we introduce a new method to compute  $t$  as a discretization problem.

### 3.5 Discrete formalism: piecewise action

We have seen that the problem described in the previous section, involving the second order variation of the magnetic action to determine the on-axis rotational transform in the continuous case leads to the operator equation Eq.(3.7). In another approach, the curve of interest can be discretized, and  $\tau$  can be determined from the Floquet exponents of the latter curve. The exponents have been shown to be linked to the residue of the curve (see Mackay and Meiss (1983) and Greene (2008)). This discrete approach is explored in what follows. Following Mackay and Meiss (1983), we consider  $n$  discretization points

$$\begin{aligned} \mathcal{S} &= \sum_{i=1}^{n-1} \int_{\mathcal{C}_i} \mathbf{A} \cdot d\mathbf{l}, \\ &= \sum_{i=1}^{n-1} S(\mathbf{x}_i, \mathbf{x}_{i+1}) \end{aligned} \quad (3.103)$$

The problem being defined here for a three dimensional periodic orbit, derivatives of the discrete action with respect to endpoints are not scalars anymore, but gradients. From now on, the following notation convention will be adopted for the derivatives:

$$\begin{aligned} \mathbf{S}_1^{[i,i+1]} &= \nabla_{\mathbf{x}_i} S^{[i,i+1]} := \nabla_{\mathbf{x}_i} S(\mathbf{x}_i, \mathbf{x}_{i+1}) \\ \mathbf{S}_2^{[i,i+1]} &= \nabla_{\mathbf{x}_{i+1}} S^{[i,i+1]} := \nabla_{\mathbf{x}_{i+1}} S(\mathbf{x}_i, \mathbf{x}_{i+1}) \end{aligned} \quad (3.104)$$

For a discretized curve that extremizes the action, the latter has to be stationary with respect to a variation in its geometry  $\delta \mathbf{x}_i$ , and the stationarity condition can be expressed in terms of the previously defined derivatives:

$$\begin{aligned} \delta S[\delta \mathbf{x}_i] &= \left[ \nabla_{\mathbf{x}_i} S^{[i-1,i]} + \nabla_{\mathbf{x}_i} S^{[i,i+1]} \right] \cdot \delta \mathbf{x}_i = 0, \\ \iff \mathbf{S}_2^{[i-1,i]} + \mathbf{S}_1^{[i,i+1]} &= \mathbf{0}. \end{aligned} \quad (3.105)$$

Note that Eq.(3.105) holds for any  $1 \leq i \leq n$ , and the stationarity condition is expressed for each point in terms of the two nearest neighbors. Upon taking the total variation of the previous result, one obtains the following:

$$\begin{aligned} \delta \left( \mathbf{S}_2^{[i-1,i]} + \mathbf{S}_1^{[i,i+1]} \right) &= \nabla_{\mathbf{x}_{i-1}} \mathbf{S}_2^{[i-1,i]} \cdot \delta \mathbf{x}_{i-1} + \nabla_{\mathbf{x}_{i+1}} \mathbf{S}_1^{[i,i+1]} \cdot \delta \mathbf{x}_{i+1} \\ &\quad + \nabla_{\mathbf{x}_i} \left( \mathbf{S}_2^{[i-1,i]} + \mathbf{S}_1^{[i,i+1]} \right) \cdot \delta \mathbf{x}_i \\ &= \mathbf{0}, \end{aligned} \quad (3.106)$$

which we rewrite in terms of the arguments of the action as

$$\overline{\mathcal{S}}_{12}^{[i-1,i]} \cdot \delta \mathbf{x}_{i-1} + \overline{\mathcal{S}}_{21}^{[i,i+1]} \cdot \delta \mathbf{x}_{i+1} + \left( \overline{\mathcal{S}}_{22}^{[i-1,i]} + \overline{\mathcal{S}}_{11}^{[i,i+1]} \right) \cdot \delta \mathbf{x}_i = \mathbf{0}, \quad 1 \leq i \leq n, \quad (3.107)$$

where we have used the following convention  $\bar{\bar{S}}_{21}^{[i,i+1]} := \nabla_{\mathbf{x}_{i+1}} \mathbf{S}_1[i, i+1]$ . Since Eq.(3.107) is valid for any  $1 \leq i \leq n$ , it can be rewritten in a tensor form:

$$\begin{pmatrix} \left(\bar{\bar{S}}_{22}^{[01]} + \bar{\bar{S}}_{11}^{[12]}\right) & \bar{\bar{S}}_{12}^{[12]} & & \lambda^{-1} \bar{\bar{S}}_{21}^{[01]} \\ \bar{\bar{S}}_{21}^{[12]} & \left(\bar{\bar{S}}_{22}^{[12]} + \bar{\bar{S}}_{11}^{[23]}\right) & \bar{\bar{S}}_{12}^{[23]} & \\ & \bar{\bar{S}}_{21}^{[23]} & \ddots & \ddots \\ & & \ddots & \ddots \\ & & & \bar{\bar{S}}_{12}^{[n-1,n]} \\ \lambda \bar{\bar{S}}_{12}^{[n,n+1]} & & \bar{\bar{S}}_{21}^{[n-1,n]} & \left(\bar{\bar{S}}_{22}^{[n-1,n]} + \bar{\bar{S}}_{11}^{[n,n+1]}\right) \end{pmatrix} \cdot \begin{pmatrix} \delta \mathbf{x}_1^T \\ \delta \mathbf{x}_2^T \\ \vdots \\ \vdots \\ \delta \mathbf{x}_{n-1}^T \\ \delta \mathbf{x}_n^T \end{pmatrix} = \mathbf{0}$$

$$\iff \begin{pmatrix} [3 \times 3] & [3 \times 3] & & [3 \times 3] \\ [3 \times 3] & \ddots & \ddots & \\ & \ddots & \ddots & \\ & & \ddots & [3 \times 3] \\ [3 \times 3] & & [3 \times 3] & [3 \times 3] \end{pmatrix} \cdot \begin{pmatrix} [3 \times 1] \\ \vdots \\ \vdots \\ [3 \times 1] \end{pmatrix} = \mathbf{0} \quad (3.108)$$

$$\iff \bar{\bar{M}}(\lambda) \cdot \delta \mathbf{x} = \mathbf{0},$$

where the block-tridiagonal form for the matrix  $\bar{\bar{M}}$  arises naturally. Note that in Mackay and Meiss (1983), the matrix was tridiagonal. The blank spaces in  $\bar{\bar{M}}$  are blocks of 0. Note that each block in  $\bar{\bar{M}}$  is of size  $3 \times 3$  since the  $\bar{\bar{S}}_{lm}$  contain the second derivatives of a 3-dimensional integral. Thus, discretizing the curve  $\mathcal{C}$  with  $n$  points,  $\bar{\bar{M}} \in \mathcal{M}_{3n \times 3n}$ , and  $\delta \mathbf{x}$  is a  $3n$  elements column vector. The  $\lambda$  denote the exponents of the curve. For Eq.(3.109) to hold, the determinant of  $M$  ought to be zero to avoid the trivial solution  $\delta \mathbf{x} = \mathbf{0}$ .

For a block tridiagonal matrix defined as follows, an expression exists to compute the determinant Molinari (2008):

$$M(z) = \begin{pmatrix} A_1 & B_1 & & z^{-1} C_0 \\ C_1 & \ddots & \ddots & \\ & \ddots & \ddots & B_{n-1} \\ z B_n & & C_{n-1} & A_n \end{pmatrix}, \quad (3.109)$$

where  $z$  is complex. It requires to define the transfer matrix  $T$ :

$$T = \prod_{i=1}^n \begin{pmatrix} -B_i^{-1}A_i & -B_i^{-1}C_{i-1} \\ \mathcal{I}_m & 0 \end{pmatrix}, \quad (3.110)$$

where  $m$  is the dimension of the square block matrices, 3 in our case, and  $\mathcal{I}_m$  the identity matrix of size  $m$ . Then,

$$\det(M(z)) = \frac{(-1)^{mn}}{(-z)^m} \det(T - z\mathcal{I}_{2m}) \det\left(\prod_{i=1}^n B_i\right). \quad (3.111)$$

Identifying the  $\lambda$  from Eq.(3.108) and Eq.(3.109) as the  $z$  from Eq.(3.111), one gets

$$\begin{aligned} \det(M(\lambda)) &= \frac{(-1)^{mn}}{(-\lambda)^m} \det(T_S - \lambda\mathcal{I}_6) \det\left(\prod_{i=1}^n \bar{\bar{S}}_{12}[i, i+1]\right) \\ T_S &= \prod_{i=1}^n \begin{pmatrix} -\bar{\bar{S}}_{12}^{-1}[i, i+1] (\bar{\bar{S}}_{22}^{[i-1, i]} + \bar{\bar{S}}_{11}^{[i, i+1]}) & -\bar{\bar{S}}_{12}^{-1}[i, i+1] \bar{\bar{S}}_{12}^{[i-1, i]} \\ \mathcal{I}_3 & 0 \end{pmatrix}. \end{aligned} \quad (3.112)$$

MacKay and Meiss use what they call a convexity condition on their Lagrangian:  $-L_{12} > 0$ , which is similar to the so-called *true angle-dynamics* from Hudson and Suzuki (2014). In our case, this can be generalized, imposing that the upper diagonal matrices are negative definite

$$\mathbf{x}^T \bar{\bar{S}}_{12}^{[i, i+1]} \mathbf{x} < 0, \quad \mathbf{x} \in \mathbb{R}^3, \quad 1 \leq i \leq n. \quad (3.113)$$

Thus, we ensure that they're invertible and that the determinant for the eigenvalue equation can indeed be computed. The multipliers  $\lambda$  are then given by the solutions of:

$$(-\lambda)^{-m} \cdot \det(T_S - \lambda\mathcal{I}) \det\left(\prod_{i=1}^n \bar{\bar{S}}_{12}[i, i+1]\right) = 0, \quad (3.114)$$

so the multipliers are nothing but the eigenvalues of the transfer matrix. The strength of this method resides in the fact that the problem is reduced to finding the eigenvalues of a  $6 \times 6$  matrix. Increasing the number of discretization points increases the size of the operator matrix  $M$ , but of interest are solely the eigenvalues of the transfer matrix.

This method is very flexible in the sense that the type of discretization that can be done for the curve  $\mathcal{C}$  is free. If  $\mathcal{C}$  can be decomposed in  $n$  sub-curves, there are several ways to define these curves. In the following section, we decide to compute explicitly the terms that appear in Eq.(3.114) for a curve discretized by piece-wise linear functions.

### 3.5.1 Particular case: piecewise linear

Taking in particular the finite paths  $\mathcal{C}_i$  to be segments, the action sums up to a sum of integral along piecewise linears  $\mathcal{C}_i := \{\mathbf{x} = \zeta(\mathbf{x}_{i+1} - \mathbf{x}_i) + \mathbf{x}_i | \zeta \in [0, 1]\}$ , the action can be decomposed as

$$\begin{aligned}\mathcal{S} &= \sum_{i=1}^{n-1} S(\mathbf{x}_i, \mathbf{x}_{i+1}), \\ S(\mathbf{x}_i, \mathbf{x}_{i+1}) &= \int_0^1 \mathbf{A}(\zeta(\mathbf{x}_{i+1} - \mathbf{x}_i) + \mathbf{x}_i) \cdot (\mathbf{x}_{i+1} - \mathbf{x}_i) d\zeta \\ &= \int_0^1 \mathbf{A}(\mathbf{v}(\mathbf{x}(\zeta))) \cdot \mathbf{u} d\zeta,\end{aligned}\tag{3.115}$$

with  $\mathbf{x}(0) = \mathbf{x}_i$  and  $\mathbf{x}(1) = \mathbf{x}_{i+1}$ , and the vector fields  $\mathbf{u}$  and  $\mathbf{v}$  defined as follows:

$$\begin{aligned}\mathbf{u}(\mathbf{x}_i, \mathbf{x}_{i+1}) &= \mathbf{x}_{i+1} - \mathbf{x}_i \\ \mathbf{v}(\zeta, \mathbf{x}_i, \mathbf{x}_{i+1}) &= \zeta(\mathbf{x}_{i+1} - \mathbf{x}_i) + \mathbf{x}_i\end{aligned}\tag{3.116}$$

such that  $\nabla_{\mathbf{x}_i} \mathbf{u}(\mathbf{x}_i, \mathbf{x}_{i+1}) = -\mathbb{1}$ ,  $\nabla_{\mathbf{x}_{i+1}} \mathbf{u}(\mathbf{x}_i, \mathbf{x}_{i+1}) = \mathbb{1}$ ,  $\nabla_{\mathbf{x}_i} \mathbf{v}(\zeta, \mathbf{x}_i, \mathbf{x}_{i+1}) = (1 - \zeta)\mathbb{1}$ ,  $\nabla_{\mathbf{x}_{i+1}} \mathbf{v}(\zeta, \mathbf{x}_i, \mathbf{x}_{i+1}) = \zeta\mathbb{1}$ .

Since

$$\begin{aligned}\nabla_{\mathbf{x}_i} \left[ \mathbf{A}(\mathbf{v}(\mathbf{x}_i)) \cdot \mathbf{u}(\mathbf{x}_i) \right] &= J_{\mathbf{A} \circ \mathbf{v}}^T(\mathbf{x}_i) \cdot \mathbf{u}(\mathbf{x}_i) + J_{\mathbf{u}}^T(\mathbf{x}_i) \cdot \mathbf{A}(\mathbf{v}(\mathbf{x}_i)) \\ &= \left[ J_{\mathbf{v}}^T(\mathbf{x}_i) \cdot J_{\mathbf{A}}^T(\mathbf{v}(\mathbf{x}_i)) \right] \cdot \mathbf{u}(\mathbf{x}_i) + J_{\mathbf{u}}^T(\mathbf{x}_i) \cdot \mathbf{A}(\mathbf{v}(\mathbf{x}_i)),\end{aligned}\tag{3.117}$$

where  $J_{\mathbf{a}}^T$  stands for the transpose of the jacobian matrix of the vector field  $\mathbf{a}$

$$\begin{aligned}\mathbf{S}_1^{[i, i+1]} &= \int_0^1 (1 - \zeta) J_{\mathbf{A}}^T(\zeta(\mathbf{x}_{i+1} - \mathbf{x}_i) + \mathbf{x}_i) \cdot (\mathbf{x}_{i+1} - \mathbf{x}_i) \\ &\quad - \mathbf{A}(\zeta(\mathbf{x}_{i+1} - \mathbf{x}_i) + \mathbf{x}_i) d\zeta\end{aligned}\tag{3.118}$$

$$\begin{aligned}\mathbf{S}_2^{[i-1, i]} &= \int_0^1 \zeta J_{\mathbf{A}}^T(\zeta(\mathbf{x}_i - \mathbf{x}_{i-1}) + \mathbf{x}_{i-1}) \cdot (\mathbf{x}_i - \mathbf{x}_{i-1}) \\ &\quad + \mathbf{A}(\zeta(\mathbf{x}_i - \mathbf{x}_{i-1}) + \mathbf{x}_{i-1}) d\zeta\end{aligned}\tag{3.119}$$

Therefore, differentiating the above expressions with respect to the appropriate arguments:

$$\begin{aligned}
 \bar{\bar{S}}_{12}^{[i-1,i]} &= \int_0^1 d\zeta \zeta \left[ (1-\zeta) \nabla_{\mathbf{v}} J_{\mathbf{A}}^T(\mathbf{v}) \cdot (\mathbf{x}_i - \mathbf{x}_{i-1}) - J_{\mathbf{A}}^T(\mathbf{v}) \right] + (1-\zeta) J_{\mathbf{A}}(\mathbf{v}) \\
 \bar{\bar{S}}_{22}^{[i-1,i]} &= \int_0^1 d\zeta \zeta \left[ \zeta \nabla_{\mathbf{v}} J_{\mathbf{A}}^T(\mathbf{v}) \cdot (\mathbf{x}_i - \mathbf{x}_{i-1}) + (J_{\mathbf{A}}(\mathbf{v}) + J_{\mathbf{A}}^T(\mathbf{v})) \right] \\
 \bar{\bar{S}}_{21}^{[i,i+1]} &= \int_0^1 d\zeta (1-\zeta) \left[ \zeta \nabla_{\mathbf{v}} J_{\mathbf{A}}^T(\mathbf{v}) \cdot (\mathbf{x}_{i+1} - \mathbf{x}_i) + J_{\mathbf{A}}^T(\mathbf{v}) \right] + \zeta J_{\mathbf{A}}(\mathbf{v}) \\
 \bar{\bar{S}}_{11}^{[i,i+1]} &= \int_0^1 d\zeta (1-\zeta) \left[ (1-\zeta) \nabla_{\mathbf{v}} J_{\mathbf{A}}^T(\mathbf{v}) \cdot (\mathbf{x}_{i+1} - \mathbf{x}_i) - (J_{\mathbf{A}}(\mathbf{v}) + J_{\mathbf{A}}^T(\mathbf{v})) \right]
 \end{aligned} \tag{3.120}$$

From the set of expressions Eq.(3.120), the transfer matrix  $\mathcal{T}_S$  can easily be implemented.

## 3.6 Conclusion

In this chapter, we combined the Floquet theory for periodic curves to the calculus of variations applied to the magnetic action. The first section of this chapter enabled to observe that stationary curves for the magnetic action are field lines. Then, the second variation of the action was used as a starting point for the Floquet theory. We derived the second variation and wrote it in the form of an operator. Expanding this operator in Mercier coordinates proved that we can recover both the Floquet exponents and  $t_a$  from the same system of equations, showing that both are related. Then, upon changing the Mercier coordinates to the Solovev-Shafanov ones, we saw that the Floquet exponents problem can be formulated using the theory of the Hill's infinite determinant. The infiniteness of the determinant makes the exponents complicated to compute, as a solution of which we came up with a discrete formalism to compute the exponents from Lagrangian principles and the magnetic action. The infiniteness of the problem has been transformed in finding the eigenvalues of a finite dimensional, 6x6 matrix, making this method promising for computational performance.



# 4 Coil vacuum energy to reduce inter-coil forces

To keep on going with our problem of optimizing a stellarator, exposed in chapter 2, we propose to focus on the second step which is to construct coils after the surface has been determined. As said in the introduction, the coils have to fulfill several objectives, such as produce a magnetic field that minimizes the quadratic flux, with good confinement properties. It is a known fact that a larger number of coils reduces the ripple in the field and enables to achieve a better minimization of the quadratic flux  $\Phi_2$ , as defined in section 2.3. However, the coils need to be spaced enough to access the vacuum vessel, for diagnostics for example. The coils also have to minimize the forces on the structure induced by the produced field, and the forces between them. In this chapter, we propose to reduce the forces on the coils produced by themselves by penalizing the vacuum field energy.

## 4.1 The energy functional

With the general formalism of shape optimization described in chapter 1, let us now introduce the vacuum field energy, computed as the integral over all space of the squared magnetic field

$$\mathcal{E} = \frac{1}{2\mu_0} \int_{\mathbb{R}^3} d\mathbf{x}^3 B^2 = \frac{1}{2\mu_0} \int_{\mathbb{R}^3} d\mathbf{x}^3 \mathbf{B} \cdot \nabla \times \mathbf{A} = \frac{1}{2\mu_0} \int_{\mathbb{R}^3} d\mathbf{x}^3 \mathbf{j} \cdot \mathbf{A}. \quad (4.1)$$

To be consistent with the way coils are defined in Simsopt, the current is constrained over the set of coil curves  $\{C_i : i = 1, \dots, N_C\}$ , enforcing a filamentary coil description:

$$\begin{aligned} \mathcal{E} &= \frac{1}{2\mu_0} \int_{\mathbb{R}^3} d\mathbf{x}^3 \mathbf{j}(\mathbf{x}) \cdot \mathbf{A}(\mathbf{x}) \chi(\mathbf{x}) \\ &= \frac{1}{2\mu_0} \sum_{i=1}^{N_C} \oint_{C_i} I_i d\mathbf{l}_i \cdot \mathbf{A}(\mathbf{x}), \end{aligned} \quad (4.2)$$

where  $\chi(\mathbf{x}) = 0$  if  $\mathbf{x}$  is not on a coil curve  $C_i$ , and 1 otherwise. Using Eq.(4.2), it is possible to express the variation of the energy with respect to variations in the coils geometries in a shape gradient form analogous to Eq.(1.16).

Let us take the first variation of  $\mathcal{E}$ :

$$\begin{aligned}\delta\mathcal{E}[\{\delta\mathbf{x}_i\}] &= \frac{1}{2\mu_0} \sum_{i=1}^{N_C} \oint_{C_i} I_i \delta(d\mathbf{l}_i \cdot \mathbf{A}) \\ &= \frac{1}{2\mu_0} \sum_{i=1}^{N_C} \oint_{C_i} I_i \delta d\mathbf{l}_i \cdot \mathbf{A} + d\mathbf{l}_i \cdot \delta \mathbf{A} \\ &= \frac{1}{2\mu_0} \sum_{i=1}^{N_C} \oint_{C_i} I_i d\mathbf{l}_i \cdot \delta \mathbf{A} + \delta \mathbf{x}_i \cdot \nabla \mathbf{A} \cdot d\mathbf{l}_i - d\mathbf{l}_i \cdot \nabla \mathbf{A} \cdot \delta \mathbf{x}_i\end{aligned}\quad (4.3)$$

The expression can be further developed using that  $\mathbf{A}$  is determined integrating the Biot-Savart law for a set of filamentary conductors:

$$\mathbf{A}(\mathbf{x}) := \frac{\mu_0}{4\pi} \sum_{i=1}^{N_C} I_i \oint \frac{d\mathbf{l}_i}{|\mathbf{x} - \mathbf{x}_i|}. \quad (4.4)$$

Therefore, the perturbation  $\delta\mathbf{A}[\{\delta\mathbf{x}_i\}]$  reads

$$\begin{aligned}\delta\mathbf{A}(\mathbf{x}) &:= \frac{\mu_0}{4\pi} \sum_{i=1}^{N_C} I_i \oint dl \left\{ \frac{\delta\mathbf{x}'_i(l)}{|\mathbf{x} - \mathbf{x}_i|} + \frac{\mathbf{x}'_i(l)}{|\mathbf{x} - \mathbf{x}_i|^3} (\mathbf{x} - \mathbf{x}_i) \cdot \delta\mathbf{x}_i \right\} \\ &= \frac{\mu_0}{4\pi} \sum_{i=1}^{N_C} I_i \oint dl \left\{ -\frac{\delta\mathbf{x}_i(l)}{|\mathbf{x} - \mathbf{x}_i|^3} (\mathbf{x} - \mathbf{x}_i) \cdot \mathbf{x}'_i(l) + \frac{\mathbf{x}'_i(l)}{|\mathbf{x} - \mathbf{x}_i|^3} (\mathbf{x} - \mathbf{x}_i) \cdot \delta\mathbf{x}_i \right\} \\ &= \frac{\mu_0}{4\pi} \sum_{i=1}^{N_C} I_i \oint dl \left\{ (\mathbf{x}'_i \delta\mathbf{x}_i - \delta\mathbf{x}_i \mathbf{x}'_i) \cdot \nabla_{\mathbf{x}} \left( \frac{1}{|\mathbf{x} - \mathbf{x}_i|} \right) \right\}.\end{aligned}\quad (4.5)$$

Thus, the term  $\propto \delta\mathbf{A}$  in Eq.(4.3) is

$$\begin{aligned}&\frac{1}{2\mu_0} \sum_{i=1}^{N_C} \oint_{C_i} d\mathbf{l}_i \cdot \delta \mathbf{A} \\ &= \frac{1}{8\pi} \sum_i \sum_j I_i I_j \oint_{C_i} \oint_{C_j} d\mathbf{l}_i \cdot \left\{ (\mathbf{x}'_j \delta\mathbf{x}_j - \delta\mathbf{x}_j \mathbf{x}'_j) \cdot \nabla_{\mathbf{x}_i} \left( \frac{1}{|\mathbf{x}_i - \mathbf{x}_j|} \right) \right\} \\ &= \frac{1}{2\mu_0} \sum_j \oint_{C_j} I_j (\mathbf{x}'_j \delta\mathbf{x}_j - \delta\mathbf{x}_j \mathbf{x}'_j) : \nabla_{\mathbf{x}_j} \left( \frac{\mu_0}{4\pi} \sum_i \oint_{C_i} I_i \frac{d\mathbf{l}_i}{|\mathbf{x}_i - \mathbf{x}_j|} \right) \\ &= \frac{1}{2\mu_0} \sum_j I_j \oint_{C_j} (\delta\mathbf{x}_j \cdot \nabla \mathbf{A}(\mathbf{x}_j) d\mathbf{l}_j - d\mathbf{l}_j \cdot \nabla \mathbf{A}(\mathbf{x}_j) \cdot \delta d\mathbf{l}_j).\end{aligned}\quad (4.6)$$

Finally, the energy perturbation is given by

$$\begin{aligned}\delta\mathcal{E} &= \frac{1}{2\mu_0} \sum_i I_i \oint_{C_i} (\delta\mathbf{x}_i \cdot \nabla\mathbf{A} \cdot d\mathbf{l}_i - d\mathbf{l}_i \cdot \nabla\mathbf{A} \cdot \delta\mathbf{x}_i) \\ &= \frac{1}{2\mu_0} \sum_i I_i \oint_{C_i} d\mathbf{l}_i \times \mathbf{B} \cdot \delta\mathbf{x}_i \\ &= \frac{1}{2\mu_0} \sum_i \oint_{C_i} (\mathbf{j} \times \mathbf{B}) \cdot \delta\mathbf{x}_i.\end{aligned}\quad (4.7)$$

Thus, the energy shape gradient  $\tilde{\mathcal{G}}_i \equiv \mathbf{j} \times \mathbf{B}$  corresponds to the force, as expected. Exploiting the properties of the vector triple product, Eq.(4.7) can be rewritten as

$$\delta\mathcal{E}[\{\delta\mathbf{x}_i\}] = \sum_i I_i \oint_{C_i} dl (\delta\mathbf{x}_i \times \mathbf{t}) \cdot \mathbf{B}, \quad (4.8)$$

which, upon comparing with Eq.(1.15) enables to identify the other form of the shape gradient as  $\mathcal{G}_i \equiv I_i \mathbf{B}$ .

As of the parameter derivatives, they are the quantities of interest since they will be implemented numerically to optimize for the shape of the coils. Using Eq.(4.8) together with Eqs.(1.19)-(1.20), the parameter derivatives of the energy functional are:

$$\frac{\partial\mathcal{E}}{\partial\Omega_k} = \sum_i I_i \oint_{C_i} dl \left( \frac{\partial\mathbf{x}_i}{\partial\Omega_k} \times \mathbf{t} \right) \cdot \mathbf{B} \quad (4.9)$$

One can also note, from the same reasoning, starting from Eq.(1.18), that the parameter derivatives can be expressed as follows:

$$\begin{aligned}\frac{\partial\mathcal{E}}{\partial\Omega_k} &= \sum_i I_i \oint_{C_i} dl (\mathbf{t} \times \mathbf{B}) \cdot \frac{\partial\mathbf{x}_i}{\partial\Omega_k} \\ &= \sum_i \oint_{C_i} (\mathbf{j}_i \times \mathbf{B}) \cdot \frac{\partial\mathbf{x}_i}{\partial\Omega_k},\end{aligned}\quad (4.10)$$

The coils geometries can be described by 3D-curves. As an illustration, a 3D curve can be written in Cartesian coordinates

$$\begin{aligned}x(\phi) &= \sum_n x_n^c \cos(n \cdot \phi) + x_n^s \sin(n \cdot \phi) \\ y(\phi) &= \sum_n y_n^c \cos(n \cdot \phi) + y_n^s \sin(n \cdot \phi) \\ z(\phi) &= \sum_n z_n^c \cos(n \cdot \phi) + z_n^s \sin(n \cdot \phi),\end{aligned}\quad (4.11)$$

where  $\phi \in [0, 2\pi]$  denotes a parameter to describe the curve. Therefore, the derivatives of the position along the curve with respect to the Fourier coefficients of the latter,

in Cartesian coordinates, can be implemented as an order 3 tensor, whose first index represents the cartesian coordinate, the second the toroidal angle, and the third the Fourier coefficient:

$$\frac{\partial \mathbf{x}_C}{\partial \Omega}(\phi) \equiv \left\{ \frac{\partial x_C^i}{\partial \Omega_j}(\phi_k) \right\}_{jk}^i \quad i \in \{1, 2, 3\}, \quad j \in \{1, 2, \dots, N\}, \quad k \in \{1, 2, \dots, N_p\}. \quad (4.12)$$

It is important to note that by definition, the energy is singular because of the integration of the fields  $\mathbf{A}$  and  $\mathbf{B}$  along the coils, fields being produced by the coils themselves. Therefore, we need to come up with an alternative to bypass the singularities of the energy, and its divergence to infinity, which is only due to a poor choice of representation, and is not physical at all. We will deal with that in subsection 4.3, and hence speak of a pseudo-energy minimization. The shape optimization for the coils, introducing the pseudo-energy as a new penalty in the functional for the optimization problem, will be carried out using the Simsopt code, described in the next section.

## 4.2 The Simsopt code

The Simsopt code is an ensemble of frameworks designed for stellarator optimization (see Landreman et al. (2021)). It comprises interfaces to existing MHD equilibrium codes, as SPEC or VMEC, as well as tools to define objective functionals to optimize for. Most geometric objects needed to carry out an optimization have been coded, such as curves, surfaces and so on. In order to design coils, let us focus on the functional optimisation tools from Simsopt.

### 4.2.1 Functional optimization

In this thesis, the Simsopt code has been used extensively to minimize a given functional, sum of several terms. The problem can be formulated as follows. We are given the functional  $\mathcal{F}$  to minimize,

$$\mathcal{F} = \sum_{i=1}^N \omega_i \mathcal{F}_i, \quad (4.13)$$

where the  $\omega_i$  are weights and the  $\mathcal{F}_i$  are functionals representing figures of merit such as the quadratic flux, the total coil length, the mean squared curvature etc. Then its differential  $d\mathcal{F}$  reads

$$d\mathcal{F} = \sum_i \omega_i d\mathcal{F}_i, \quad (4.14)$$

and simsopt will compute at each iteration of the optimization algorithm the derivatives of  $\mathcal{F}$  with respect to the DOFs of the system, which are an input. The result is then used

by the L-BFGS-B algorithm that evaluates the gradient of the functional to determine the steepest descent direction.

#### 4.2.2 L-BFGS-B algorithm and Jacobian vector product

Let us briefly describe the L-BFGS-B algorithm: Initially designed to solve the following problem,

$$\begin{aligned} & \min_{\mathbf{x}} f(\mathbf{x}) \\ & \mathbf{l}_b \leq \mathbf{x} \leq \mathbf{u}_b, \end{aligned} \tag{4.15}$$

with  $\mathbf{l}_b$  and  $\mathbf{u}_b$  the lower and upper bounds respectively of the vector  $\mathbf{x}$ , it has been proven to be very efficient in solving unconstrained problems such as Eq.(4.16) (Zhu et al. (1997)). The only information that has to be provided by the user is the gradient, and the hessian matrix is not required, which is advantageous since it can be seemingly heavy to compute for large number of variables with large number of degrees of freedom. At each iteration, a limited memory *approximation of the hessian* is given. Since the hessian is related to the extrema of a functional (saddle points and local extrema), this limited memory matrix enables to define a quadratic model for  $f$ . The search direction for the minima is then defined as the direction between the current iteration step and the *approximate minimizer*, obtained from the set of active variables. Finally, a *line search* is performed along this direction. A more detailed description of the L-BFGS-B algorithm can be found in Byrd et al. (1995).

The computational performance is increased by mean of the so called vector jacobian product, which enables to compute the full derivatives of any object with respect to the degrees of freedom of an intermediate one, without actually computing each term of the jacobian. The vector jacobian product of the energy with respect to the coils geometry and the current is given in appendix A.6

### 4.3 Pseudo-energy minimization

#### 4.3.1 Target functional

In what follows, the Simsopt code has been used to implement and minimize the vacuum field (pseudo-)energy. In this stage-two optimization problem for coil design, we consider the following functional:

$$\mathcal{F} = \Phi_2 + \omega_L \mathcal{L} + \omega_E \mathcal{E}, \tag{4.16}$$

where  $\mathcal{L} = \sum_{C_i} \mathcal{L}_i$  is the sum of the coils lengths,  $\mathcal{E}$  the energy of the system, and  $\omega_L$  and  $\omega_E$  the respective weights. As stated earlier in the description of the Simsopt framework, the gradient of each term has been implemented in the form of a vector jacobian product.

### 4.3.2 Limitations to the filamentary coil description

As explained earlier, the energy is singular because of the filamentary coil representation. To avoid the singularities, an alternative is to evaluate the magnetic field and the magnetic vector potential on a "ghost-curve", defined by displacing the coil-curve in a direction normal to the curve, either along the normal or the binormal vector, by an amount  $\epsilon \ll 1$ .

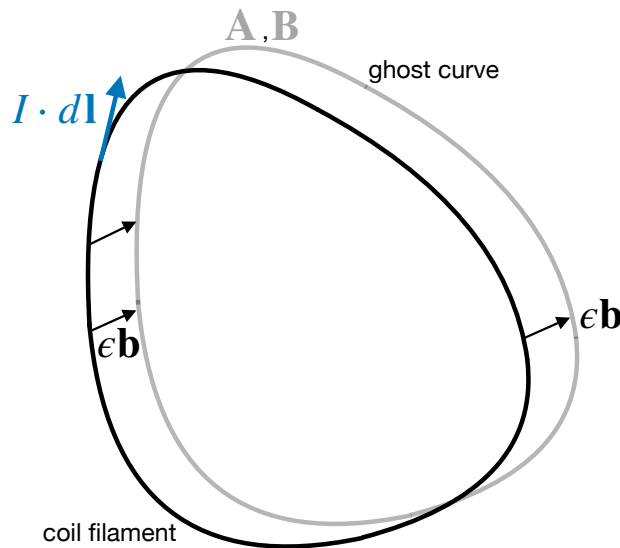


Figure 4.1 – Filamentary coil curve (black) and ghost curve defined by binormal  $\epsilon$ -displacement.

For a given coil  $C_i$  and  $\epsilon \ll 1$ , we can define a ghost curve as the following:

$$C_i^\epsilon := \{\mathbf{x} = \mathbf{x}_i + \epsilon \mathbf{a} \mid \mathbf{x}_i \in C_i, \mathbf{a} \in \{\mathbf{n}, \mathbf{b}\}\} \quad (4.17)$$

Therefore, we can define the following pseudo-energy  $E_\epsilon$ :

$$E_\epsilon := \frac{1}{2} \sum_i I_i \oint_{C_i^\epsilon} d\mathbf{l}(\mathbf{x}_i) \cdot \mathbf{A}(\mathbf{x}_i^\epsilon) \quad (4.18)$$

The energy expression Eq.(4.18) is therefore non-singular. One can ask if such an approximation for the energy is legitimate. The energy computed as a sum of loop-integrals along the curves of  $\mathbf{A}$  is singular when the field produced by a coil  $C_i$  is evaluated on itself. Therefore, the "diagonal" terms are dominant in the sense that they diverge towards infinity. Redefining the energy as Eq.(4.18) enables to overcome the singularity

### 4.3. Pseudo-energy minimization

---

problem by providing an expression that is finite for a given  $\epsilon$ , and that diverges as  $\epsilon \downarrow 0$  since it gets closer to the actual energy value.

$$E \equiv \begin{pmatrix} \infty & < \infty \\ < \infty & \infty \end{pmatrix} \quad (4.19)$$

Since the actual energy of the system is a physical quantity not supposed to vary with our choice of model, the results need to be normalized by  $\epsilon^{-1}$ . Computing the limit explicitly from Eq.(4.4):

$$\begin{aligned} \lim_{\epsilon \downarrow 0} \epsilon E_\epsilon &= \lim_{\epsilon \downarrow 0} \frac{\epsilon}{2\mu_0} \sum_i I_i \oint_{C_i^\epsilon} d\mathbf{l}(\mathbf{x}_i) \cdot A(\mathbf{x}_i^\epsilon) \\ &= \lim_{\epsilon \downarrow 0} \frac{\epsilon}{8\pi} \sum_i \sum_k \oint_{C_i} \oint_{C_k} I_i I_k \frac{d\mathbf{l}(\mathbf{x}_i) \cdot d\mathbf{l}(\mathbf{x}_k)}{|\mathbf{x}_i + \epsilon \mathbf{a} - \mathbf{x}_k|} \\ &= \frac{1}{8\pi} \sum_i I_i^2 \oint_{C_i} \oint_{C_i} d\mathbf{l}(\mathbf{x}_i) \cdot d\mathbf{l}(\mathbf{x}_i) < \infty, \end{aligned} \quad (4.20)$$

where for the last line, we used that  $\mathbf{a}$  is a unit vector. Therefore, we went from Eq.(4.19) to Eq.(4.21), where the matrix representation emphasizes the contributions to the  $E_{ik}$  terms and  $E_{\epsilon,ik}$  terms:

$$\lim_{\epsilon \downarrow 0} E_\epsilon \equiv \begin{pmatrix} < \infty & 0 \\ 0 & < \infty \end{pmatrix} \quad (4.21)$$

At this stage, we do not know yet if minimizing this pseudo-energy composed of the dominant integral terms in the actual energy definition, is going to reduce the forces on the coils. We need first to test the behavior of the code with this new target function added to the optimization formalism. At least the two following tests need to be ran:

- Convergence of the  $\epsilon \mathcal{E}_\epsilon$  as  $\epsilon \downarrow 0$ .
- Decrease of the final configuration energy values as the weight on the energy increases in Eq.(4.16)

When these two properties will have been tested for, we will start trying to reduce the forces on the coils for two magnetic configurations. The same precise QA as mentioned before, as well as the W7X configuration. This will be treated in section 4.5.

## 4.4 Implementation verifications and consistency checks

In order to verify our implementation of the pseudo energy, we carry on a series of tests for several properties to see if the code results match the expected behavior mathematical predictions. For the tests, the magnetic configuration considered is the precise QA configuration from Landreman and Paul (2022). This configuration is a 2 field period QA magnetic field. The initial coil configuration is the following:  $N = 8$  coils by field period, and the coils are equidistant and circular.

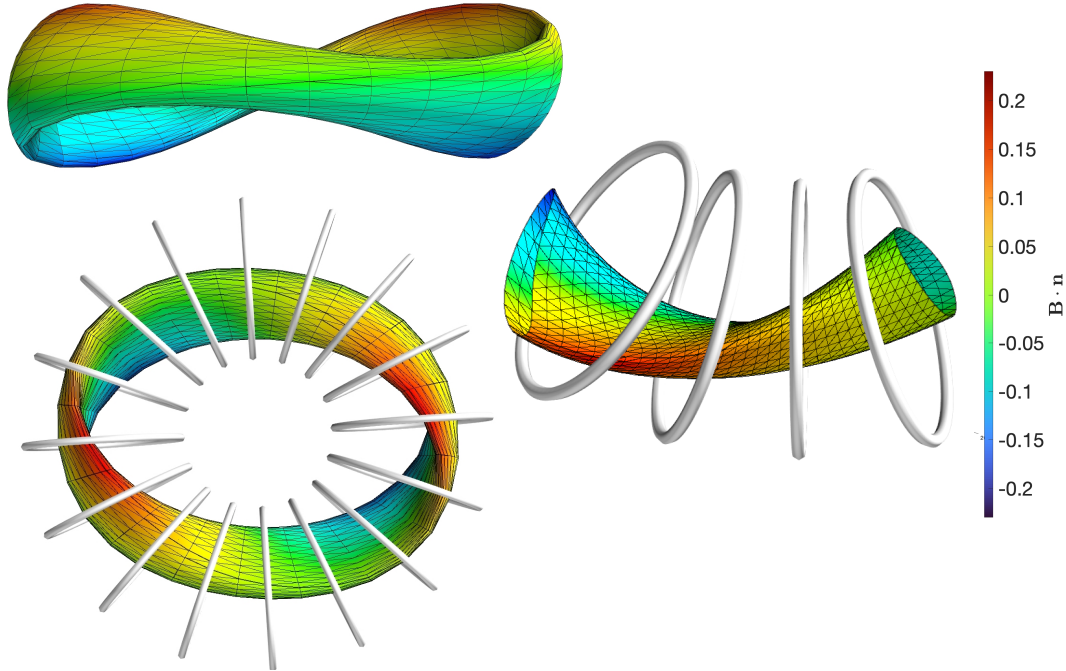


Figure 4.2 – Precise QA configuration from Landreman and Paul (2022). The initial coil configuration is shown. The right plot shows the coils on one half period, since by symmetry the optimization is carried on half a period for an increased performance.

### 4.4.1 Behavior as a function of the ghost-curve

In this subsection, we propose to verify the convergence of the energy functional as we change the ghost-curve, by making it closer to the actual close curve (taking the limit  $\epsilon \downarrow 0$ ), and by changing the displacement vector. The results are grouped in table 4.1. To produce these results, the parameters that have been chosen for the code are the following:  $N_F = 5$  the number of Fourier modes to describe the coils curves and  $N = 2 \times 4$  coils per field period.

#### 4.4. Implementation verifications and consistency checks

---

Table 4.1 –  $\epsilon \mathcal{E}_\epsilon$  for several ghost curves as  $\epsilon \downarrow 0$ .

$\epsilon$	$\epsilon \mathcal{E}(-\epsilon \mathbf{n})$	$\epsilon \mathcal{E}(+\epsilon \mathbf{n})$	$\epsilon \mathcal{E}(-\epsilon \mathbf{b})$	$\epsilon \mathcal{E}(+\epsilon \mathbf{b})$
$10^{-2}$	680.78	684.10	683.35	681.49
$10^{-3}$	299.89	299.93	299.92	299.90
$10^{-4}$	261.23	261.23	261.23	261.23
$10^{-5}$	257.36	257.36	257.36	257.36
$10^{-6}$	256.98	256.98	256.98	256.98
$10^{-7}$	256.94	256.93	256.94	256.94
$10^{-8}$	256.93	256.93	256.93	256.93
$10^{-9}$	256.93	256.93	256.93	256.93
$10^{-10}$	256.93	256.93	256.93	256.93
$10^{-11}$	256.93	256.93	256.93	256.93
$10^{-12}$	256.93	256.93	256.93	256.93
$10^{-13}$	256.94	256.94	256.93	256.93
$10^{-14}$	256.93	256.93	256.91	256.91

Analyzing the results from table 4.1, we observe that the energy of the final configuration, for a given and small-enough  $\epsilon$ , is identical up to a relative error of  $\sim 10^{-4}$ , which is in agreement with what we expected. When  $\epsilon \leq 10^{-14}$ , the relative error increases a little as we get closer to machine precision.

We also proceed to a scan of the Fourier resolution of the coils curves. We recall that the coils curves are 3 dimensional curves, described by a truncated Fourier series such as

$$\mathbf{x}(\phi) = \sum_{n=0}^{N_F} \mathbf{x}_n^c \cos(n\phi) + \mathbf{x}_n^s \sin(n\phi), \quad (4.22)$$

where  $\mathbf{x}_n^c$  and  $\mathbf{x}_n^s$  contain the Fourier modes of the curves. Note that here again,  $\phi$  needs to be an appropriate toroidal angle, which might not be suitable for strongly shaped geometries, which can be avoided by constraining the curvature of the coils for example. Fig.(4.3) shows the result for the energy of the final configuration. As the Fourier resolution increases, the energy of the final configuration decreases. We would need to carry an expansion to higher order of the coils geometries in order to verify that the energy converges with respect to the Fourier resolution. The right plot from Fig.(4.3) shows the energy as a function of the Fourier resolution, for  $\epsilon = 10^{-9}$ .

Therefore, for the following tests and optimizations, we will fix  $\epsilon = 10^{-9}$ , which is a sufficiently low value.

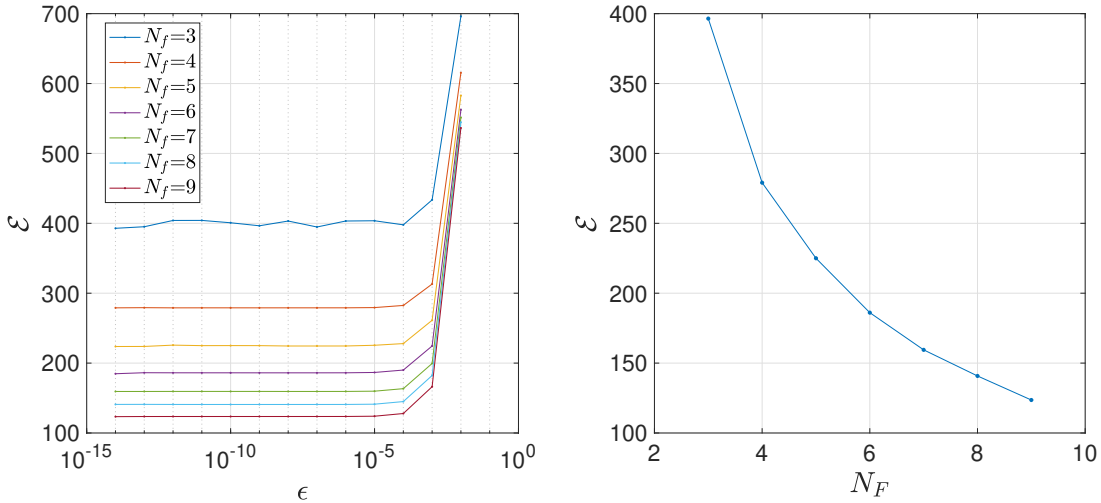


Figure 4.3 – Left: Scan of the final energy as a function of  $\epsilon$  the ghost-curve parameter, for several curves' Fourier resolution  $N_F$  - Right:  $\mathcal{E}(N_F)$  for  $\epsilon = 10^{-9}$ .

#### 4.4.2 Increasing the penalty on the energy

In this subsection, we focus on the behavior of the code in the computation of configurations as we increase the penalty on the energy, leaving the weights on  $\Phi_2$  and  $\mathcal{L}$  fixed. We recall that increasing the weight of a given quantity in the target functional Eq.(4.13) should lead to a decrease in the final value of the quantity in question, and an increase in the others, if their weight has been kept fixed.

Still with the same QA configuration as a starting point, with  $N = 8$  coils per field period and  $\epsilon = 10^{-9}$ , we proceed to a scan over several values of the energy weight  $\omega_E$  keeping the weight on the length fixed (and the one on the quadratic flux too). Fig.(4.4) shows the result for  $\omega_E$  ranging between  $10^{-12}$  and  $10^{-7}$ , for ghost curves defined by normal and binormal displacement. In the low  $\omega_E$  values, the code seems not to be efficient since for the first few points the energy increases. The same behavior is observed in the higher values of  $\omega_E$ . In the middle range, the energy seems to behave properly.

However, we expected the curve to be smooth. Somehow, it exhibits a sawtooth shape in some ranges. As of now, the author can not explain this behavior of the energy curve. Some more studies need to be done. However, we can emit hypotheses:

- Certainly comes from the fact that the way the energy is computed is an approximation that has been made to overcome the fact that when it comes to magnetic field and self-forces, the filamentary description is a poor choice. For a better description, that does not take into account only the "diagonal" dominant terms, one might need to add some thickness to the coils, in order to compute the magnetic field on the coils (Landreman et al. (2023)).

#### 4.4. Implementation verifications and consistency checks

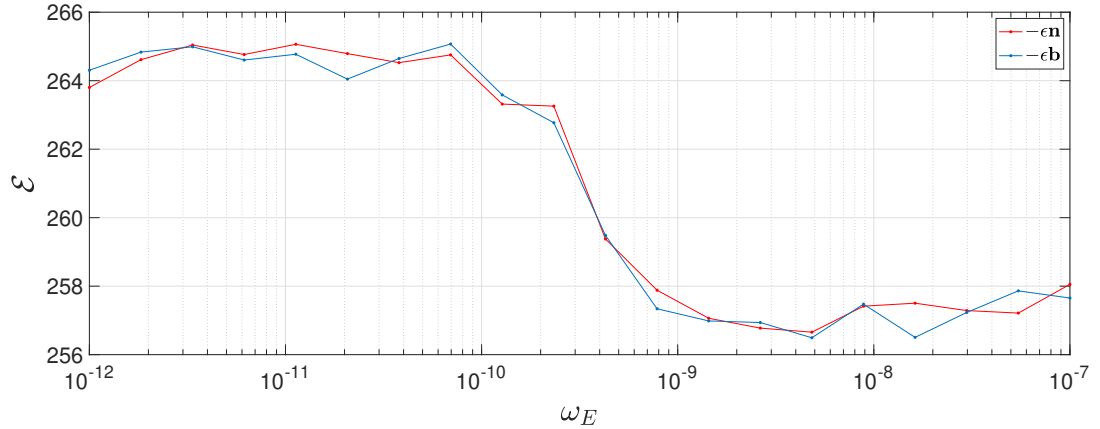


Figure 4.4 – Final configuration energy for two types of ghost curves, as a function of the weight  $\omega_E$ .

- The normal and binormal vectors show some discontinuities in their orientation along the coil curves as the coils get more strongly shaped. See Fig.(4.5).
- Might come from the Fourier resolution for the curves. However, Fig.(4.3) shows that the energy as a function of the Fourier resolution shows similar trend for fixed values of  $\epsilon$ . Still it could be investigated.
- Since the L-BFGS-B algorithm is a non-linear optimization algorithm, the weights of either the length or the quadratic flux might have to be adapted too. They have been kept fixed, but they might need to be of the form  $\omega_i \equiv \omega_i(\omega_E)$ .

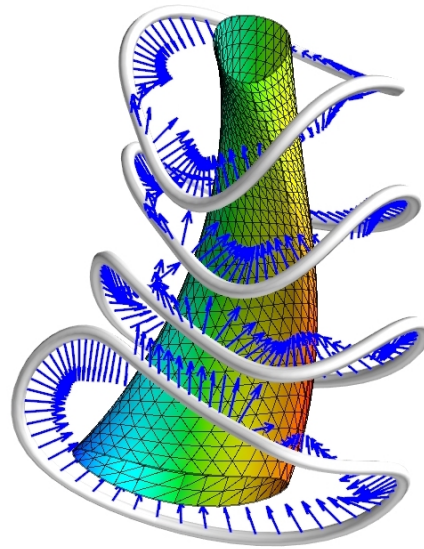


Figure 4.5 – Half a field period from the QA configuration with coils designed by penalizing  $\Phi_2$  and  $\mathcal{L}$ . The normal vector from the Frenet frame is plotted in blue along the coils.

## 4.5 Results

Now that the code has been tested, we can focus on designing stellarator coils and study the impact of penalizing the vacuum energy on the coils forces. We will conduct this study on two magnetic configurations: the precise QA and W7X.

### 4.5.1 Precise QA configuration

We start by the precise QA configuration from Landreman and Paul (2022). In order to test whether penalizing the vacuum energy enables to indeed reduce the forces on the coils, we compare the forces on each coil in a case where the penalty on the energy is very low, and one where the penalty is higher, targeting the same value for  $\Phi_2$ . Fig.(4.6) shows the result for half a period. The quiver plot represents the  $\mathbf{j} \times \mathbf{B}$  force on each coil. It seems that the max force reached on each coil is a little bit lower in the case where the penalty on the energy was very low, which is so far, not in the favor of penalizing the energy. However, the peak force is of the same order of magnitude. Therefore, we want to be able to compare the integrated force along each coil - the total force

$$F_i^t = \oint_{C_i} |\mathbf{j} \times \mathbf{B}| dl. \quad (4.23)$$

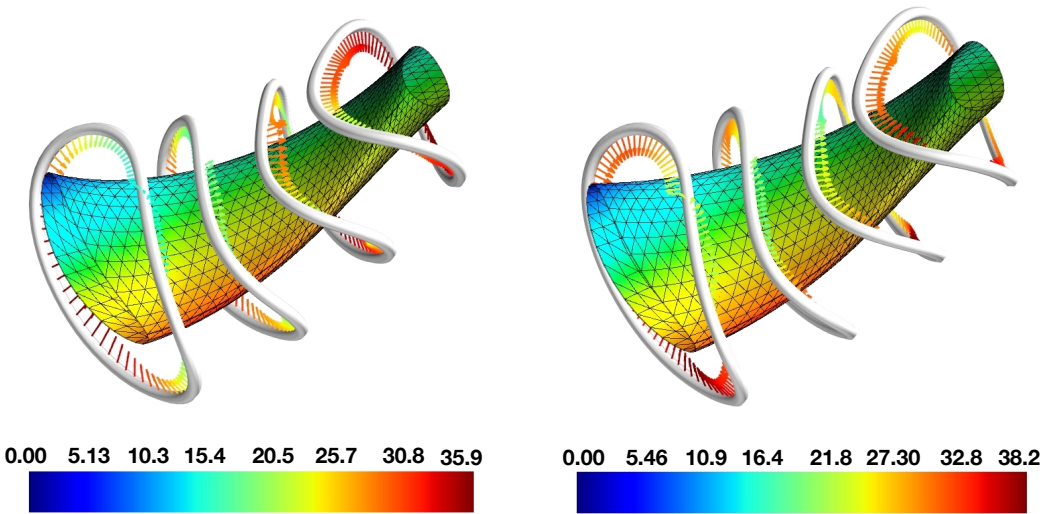


Figure 4.6 – Half a period of the precise QA configuration with coils obtained from Simsopt. Left:  $\omega_E = 10^{-12}$  - Right:  $\omega_E = 10^{-7}$  - The units are arbitrary

The results for the integrated forces  $F_i^t$  are given in table(4.2). One notes that although the peaked force is higher in the case where the penalty on the energy is greater, the integrated forces are lower. Therefore, penalizing the vacuum energy is favorable in order to reduce the average forces on the coils.

Table 4.2 – Integrated  $\mathbf{j} \times \mathbf{B}$  force along the coils for two distinct penalties on  $\mathcal{E}$  - QA

$\int_{C_i}  \mathbf{j} \times \mathbf{B}  dl$	$\omega_E = 10^{-12}$	$\omega_E = 10^{-7}$
coil 1	113.70	102.80
coil 2	101.04	98.06
coil 3	92.02	90.30
coil 4	84.48	84.15

The resulting set of coils (optimization conducted with  $\omega_E = 10^{-7}$ ) is represented in Fig.(4.7). However, one might argue that the forces are not reduced a whole lot (the maximum reduction is  $\sim 10\%$ ). As a next step, to see if the forces can be further reduced by penalizing the energy, it will be necessary to have a better model for the energy of the coils, by introducing a non-zero thickness. As of today, such a feature does not exist in the simopt framework, but so far, the results are encouraging.

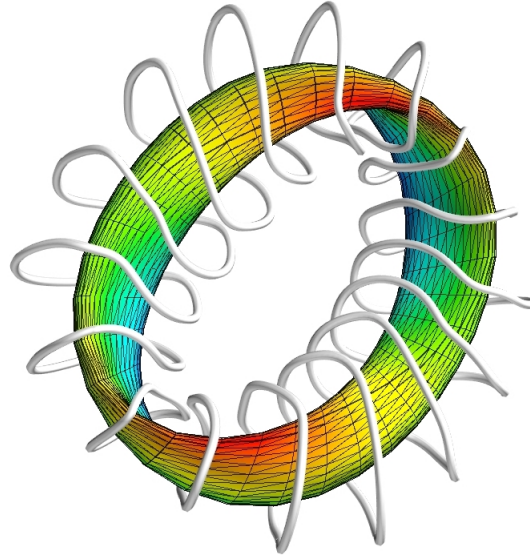


Figure 4.7 – Precise QA configuration with optimized coils penalizing the vacuum energy.

It might be interesting to have a look at a stellarator configuration that has been actually built. The following section will be dedicated to the W7X stellarator, located in Greifswald (Germany), which is the first stellarator built that has shown promising results for fusion produced energy.

#### 4.5.2 The W7X configuration

The Wendelstein-7-X magnetic configuration is depicted in Fig.(4.9). It is a 5 field-periods stellarator, with major radius  $R_0 = 5.5\text{m}$  and minor radius  $R_1 = 0.53\text{m}$ . The plasma volume is  $\sim 30$  cubic meters and the magnetic field reaches 3T. W7X has 10 coils per field period. W7X was designed combining results from the MHD equilibrium code VMEC and coils optimized with a coil-design code using a virtual casing principle (Lumsdaine et al. (2016), Hanson (2015)). We want to see if introducing a penalty on the vacuum energy can also help lower the forces. Since the author did not have access to the actual W7X coils geometry, we conducted the same study as the one in the previous subsection dedicated to the QA configuration, starting from circular coils.

The results for the  $\mathbf{j} \times \mathbf{B}$  force along each coil on half a field period are shown in Fig.(4.8). As in the previous QA case, the peak forces are higher in the case of a higher penalty. Results for the integrated forces are depicted in table(4.3). However, here again, the forces were reduced between a lower penalty and a higher one by at most  $\sim 6\%$ .

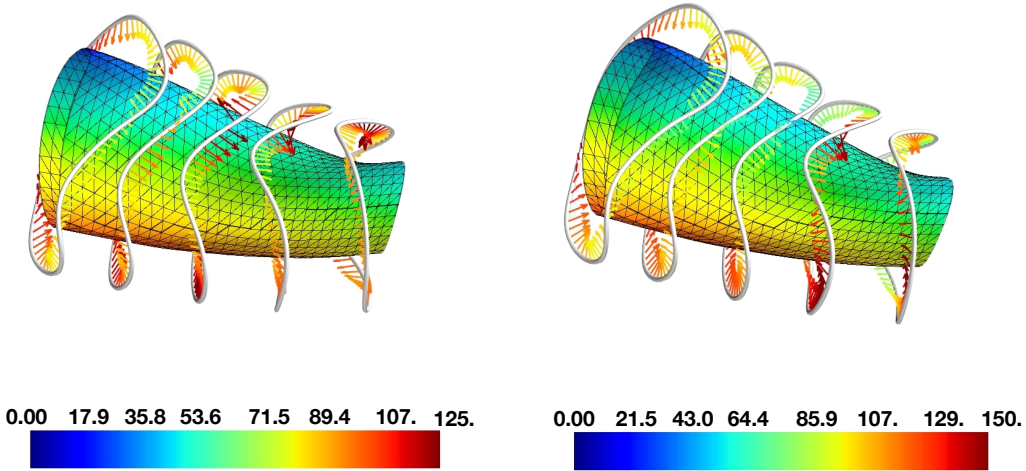


Figure 4.8 – Half a period of W7X with coils obtained from Simsopt. Left:  $\omega_E = 10^{-12}$  - Right:  $\omega_E = 10^{-7}$  - The units are arbitrary.

Table 4.3 – Integrated  $\mathbf{j} \times \mathbf{B}$  force along the coils for two distinct penalties on  $\mathcal{E}$  - W7X

$\int_{C_i}  \mathbf{j} \times \mathbf{B}  dl$	$\omega_E = 10^{-12}$	$\omega_E = 10^{-7}$ - W7X
coil 1	736.3	730.6
coil 2	721.3	705.9
coil 3	733.6	695.6
coil 4	725.7	698.6
coil 5	741.2	696.3

The coils resulting from the optimization with higher energy weight are given in Fig.(4.9).

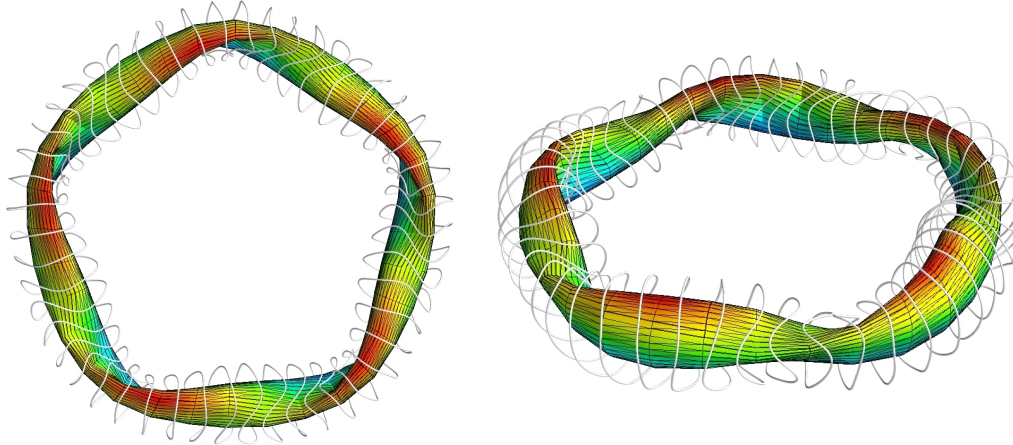


Figure 4.9 – W7X configuration with optimized coils penalizing the vacuum energy and obtained with Simsopt.

### 4.5.3 Summary

In the above chapter, we have introduced the vacuum field energy as a functional to optimize for in the stellarator coil design framework. We developed its mathematical expression to show that its shape gradient is indeed the  $\mathbf{j} \times \mathbf{B}$  force. We have shown that in the case where the coils are described by filaments, with 0 thickness, the model for the energy breaks down as it is singular since the fields are singular on the coils. We have then introduced an alternative expression for the energy, that comprises the terms that are dominant because divergent, and make it converge by mean of ghost curves to evaluate the fields on. This being done, we tested our implementation of this pseudo-energy before running the code to actually try to reduce the forces on the coils. We have seen that penalizing more the energy, by targeting the same final value of  $\Phi_2$  led to higher peak forces but lower integrated force  $F^t$ . This result is very encouraging for future investigations to reduce the forces on the coils and on the structure around the stellarator. This might be done by taking into account the effective coil-thickness for example.



# 5 Conclusion and futures perspectives

In this thesis, we set the bases for an Euler-Lagrange equation for an optimized stellarator, with as final goal, to be one single equation that is verified by an optimal configuration. This would have as potential application to help mapping the space of optimized configurations maybe more efficiently than scanning numerically large parameter spaces (Landreman (2022)).

However, we noticed that determining an equation for an optimized stellarator involves expressing the variation of each quantity in the same surface variation form, which can be very challenging when the functional depends on intermediate quantity such as the magnetic axis. Therefore, we were not able to express the variation of the Floquet exponents (hence the on-axis rotational transform) in a surface shape-gradient form.

On the other hand, optimizing a stellarator involves constructing a set of coils that verify a certain amount of properties. Among those, the forces on the coils themselves and on the surrounding structure need not to be too high. In order to reduce those forces and hence the stress on the structure, we proposed to reduce the integral of the magnetic field outside of the target plasma volume. The coils forces were shown to be lower, but not by much.

## 5.1 Future perspectives

Although some progress has been made in the description of magnetic field lines via Floquet theory, we limited our study to the magnetic axis, in order to compute  $\tau$ . However, we have shown that the nature of the exponents, being real or complex was determining if the curve would be around an O point or an X point. For a future work, we consider extending our study to periodic curves in the neighborhood of rational surfaces to try to describe how islands can be opened. Moreover, we'll try to describe the behavior of curves next to an X point, since this might have applications in the design of divertors for stellarators.

Regarding the Euler-Lagrange equation, the variation of the rotational transform  $\delta t_a$  needs to be expressed in a surface shape gradient form, as well as the amount of rotational transform that can be produced by unit energy  $\delta t_a/\delta \mathcal{E}$ .

As of the coil design problem, this thesis enabled us to show that although the filamentary coil description is suitable enough to optimize for coils with objective functions as magnetic fluxes, coil to coil separation, coils curvature, torsion and so on, consider that the coils have a zero thickness is not working when we try to implement the energy, and in a more general case, when the fields need to be evaluated on the coils. To solve this issue, we hope to be able in a future work to add to the Simsopt framework a non-zero thickness for the coils, so the energy can be computed accurately.

In addition, we might want to express or parametrize the coil-design problem differently, including different or more penalties in the target functional.

# A Appendices

## A.1 Derivation of the transport theorems

Let us consider the two following functionals, depending on the volume  $V$  defined by the closed bounded surface  $\partial V = S$ :

$$\begin{aligned} J_1(V) &:= \int_V d\mathbf{x}^3 j_1(\mathbf{x}) \\ J_2(V) &:= \int_S d\mathbf{x}^2 j_2(\mathbf{x}). \end{aligned} \tag{A.1}$$

Noting that the transformation from  $V \rightarrow V_\epsilon$ , where  $V_\epsilon := \{\mathbf{x}_\epsilon : \mathbf{x}_\epsilon = \mathbf{x} + \epsilon \nabla \delta \mathbf{x} \mid \mathbf{x} \in V\}$  has jacobian  $\mathcal{I} + \epsilon \nabla \delta \mathbf{x}$ , we can express the shape derivative of the volume integrated functional  $J_1$  as follows:

$$\begin{aligned} \delta J_1[\delta \mathbf{x}] &= \lim_{\epsilon \downarrow 0} \left\{ \frac{J_1(V_\epsilon) - J_1(V)}{\epsilon} \right\} \\ &= \lim_{\epsilon \downarrow 0} \frac{1}{\epsilon} \left\{ \int_{V_\epsilon} d\mathbf{x}^3 j_1(\mathbf{x}) - \int_V d\mathbf{x}^3 j_1(\mathbf{x}) \right\} \\ &= \lim_{\epsilon \downarrow 0} \frac{1}{\epsilon} \left\{ \int_V d\mathbf{x}^3 j_1(\mathbf{x} + \epsilon \nabla \delta \mathbf{x}) \det(\mathcal{I} + \epsilon \nabla \delta \mathbf{x}) - \int_V d\mathbf{x}^3 j_1(\mathbf{x}) \right\}. \end{aligned} \tag{A.2}$$

Moreover,  $j_1(\mathbf{x} + \epsilon \nabla \delta \mathbf{x}) = j_1(\mathbf{x}) + \epsilon \delta j_1(\mathbf{x}) + \epsilon \delta \mathbf{x} \cdot \nabla j_1(\mathbf{x}) + \mathcal{O}(\epsilon^2)$ , which enables to write

$$\begin{aligned} \delta J_1[\delta \mathbf{x}] &= \lim_{\epsilon \downarrow 0} \frac{1}{\epsilon} \left\{ \int_V d\mathbf{x}^3 \det(\mathcal{I} + \epsilon \nabla \delta \mathbf{x}) \left( j_1(\mathbf{x}) + \epsilon \delta j_1(\mathbf{x}) + \epsilon \delta \mathbf{x} \cdot \nabla j_1(\mathbf{x}) + \mathcal{O}(\epsilon^2) \right) - j_1(\mathbf{x}) \right\} \\ &= \lim_{\epsilon \downarrow 0} \int_V d\mathbf{x}^3 \frac{1}{\epsilon} \left\{ \left( \det(\mathcal{I} + \epsilon \nabla \delta \mathbf{x}) - 1 \right) j_1(\mathbf{x}) \right. \\ &\quad \left. + \det(\mathcal{I} + \epsilon \nabla \delta \mathbf{x}) \left( \epsilon \delta j_1(\mathbf{x}) + \epsilon \delta \mathbf{x} \cdot \nabla j_1(\mathbf{x}) \right) + \mathcal{O}(\epsilon^2) \right\}. \end{aligned} \tag{A.3}$$

## Appendix A. Appendices

---

Making use of the fact that  $\det(\mathcal{I}) = 1$ , and of the linearity of the determinant, one can rewrite Eq.(A.3) as

$$\delta J_1[\delta \mathbf{x}] = \int_V d\mathbf{x}^3 \left\{ j_1(\mathbf{x}) \frac{d}{d\epsilon} \Big|_{\epsilon=0} \det(\mathcal{I} + \epsilon \nabla \delta \mathbf{x}) + \delta j_1(\mathbf{x}) + \delta \mathbf{x} \cdot \nabla j_1(\mathbf{x}) \right\}, \quad (\text{A.4})$$

which, together with Jacobi's formula for the derivative of the determinant with respect to  $\epsilon$ , reads

$$\begin{aligned} \delta J_1[\delta \mathbf{x}] &= \int_V d\mathbf{x}^3 \left\{ \delta j_1(\mathbf{x}) + (\nabla \cdot \delta \mathbf{x}) j_1(\mathbf{x}) + \delta \mathbf{x} \cdot \nabla j_1(\mathbf{x}) \right\} \\ &= \int_S d\mathbf{x}^2 (\delta \mathbf{x} \cdot \mathbf{n}) j_1(\mathbf{x}) + \int_V d\mathbf{x}^3 \delta j_1(\mathbf{x}), \end{aligned} \quad (\text{A.5})$$

where from the first to second line we used that  $\text{tr}\left((\mathcal{I} + \epsilon \nabla \delta \mathbf{x})^{-1}|_{\epsilon=0} \nabla \delta \mathbf{x}\right) = \text{tr}(\nabla \delta \mathbf{x}) = \nabla \cdot \delta \mathbf{x}$ . The second equality of Eq.(A.5) is often called the *Reynolds transport theorem* for volume integrated functionals. This transport theorem can be used to derive an expression for the first variation of surface integrated functionals, for which the domain of integration depends on the varied parameter.

In order to develop the second transport theorem, for the surface-integrated functional  $J_2$  from Eq.(A.1), let us first recall the definition of the signed distance function  $d_0$ :

$$d_0(\mathbf{x}) = \begin{cases} -d(\mathbf{x}, \partial V), & \mathbf{x} \in V \\ 0, & \mathbf{x} \in \partial V \\ d(\mathbf{x}, \partial V), & \mathbf{x} \in V^c \end{cases} \quad (\text{A.6})$$

where  $d(\mathbf{x}, \partial V)$  is taken as the shortest distance between  $\mathbf{x}$  and the boundary of  $V$ , with respect to the metric  $d$ :

$$d(\mathbf{x}, \partial V) := \inf_{\mathbf{y} \in \partial V} d(\mathbf{x}, \mathbf{y}). \quad (\text{A.7})$$

Thus, the normal to the surface can be expressed as  $\mathbf{n} := \nabla d_0$ , and is by definition a unit vector. By mean of the divergence theorem, we can express the second functional  $J_2$  as follows

$$J_2 = \int_V d\mathbf{x}^2 \nabla \cdot (j_2 \nabla d_0), \quad (\text{A.8})$$

---

### A.1. Derivation of the transport theorems

and use Eq.(A.5) so the variation of Eq.(A.8) reads

$$\delta J_2 = \int_S d\mathbf{x}^2 \left\{ (\delta \mathbf{x} \cdot \mathbf{n}) (\mathbf{n} \cdot \nabla j_2 + j_2 \Delta d_0) + \nabla d_0 \cdot \nabla \delta d_0 + \delta j_2 \right\} \quad (\text{A.9})$$

Upon noting that  $\nabla d_0 \cdot \nabla \delta d_0 = 1/2\delta(\nabla d_0 \cdot \nabla d_0) = 0$  since  $\nabla d_0$  remains unitary under variations of the boundary. If we define the mean curvature  $H$  as the tangential divergence of the unit normal, i.e.  $H := \nabla_\Gamma \cdot \mathbf{n}$ , Eq.(A.9) rewrites as

$$\delta J_2 = \int_S d\mathbf{x}^2 \left\{ \delta j_2 + (\mathbf{n} \cdot \nabla j_2 + 2Hj_2) (\delta \mathbf{x} \cdot \mathbf{n}) \right\}. \quad (\text{A.10})$$

A formal definition of the tangential gradient operator and some of its properties or related operators can be found in A.2

## A.2 Tangential differential operators

Following the notation of Nies et al. (2022), we introduce the several tangential differential operators useful for shape optimization. Let us start by defining the *tangential gradient*. To do so, consider the function  $f$  defined on  $\bar{V} \equiv \dot{V} \cup \partial V$ , and  $\Gamma = \partial V$ :

$$\nabla_\Gamma f := \nabla f - \mathbf{n}(\mathbf{n} \cdot f). \quad (\text{A.11})$$

It obviously satisfies  $\nabla_\Gamma f \cdot \mathbf{n} = 0$ . Note that in chapter 2, the boundary is denoted by  $S$  and not  $\Gamma$ . Now, we define the *tangential divergence operator*, acting on a vector field  $\mathbf{f}$ , defined on  $\bar{V}$  as well.

$$\nabla_\Gamma \cdot \mathbf{f} := \nabla \cdot \mathbf{f} - \mathbf{n} \cdot \nabla \mathbf{f} \cdot \mathbf{n} \quad (\text{A.12})$$

Let us finally derive the expression of the *tangential Laplace operator*  $\nabla_\Gamma \cdot \nabla_\Gamma$ , using the two operators previously introduced. To do so, let it act on the real valued continuous function  $f$ , defined on  $\bar{V}$ :

$$\begin{aligned} \nabla_\Gamma \cdot \nabla_\Gamma f &:= \Delta f - \nabla \cdot \mathbf{n}(\mathbf{n} \cdot \nabla f) - \mathbf{n} \cdot \nabla(\mathbf{n} \cdot \nabla f) - \mathbf{n}^T \cdot \mathcal{H}f \cdot \mathbf{n} \\ &\quad + \mathbf{n}^T \cdot \nabla(\mathbf{n} \mathbf{n}^T \cdot \nabla f) \cdot \mathbf{n} \\ &= \Delta f - h(\mathbf{n} \cdot \nabla f) - \cancel{\mathbf{n}^T \cdot \nabla \mathbf{n}} \cdot \nabla f - \mathbf{n}^T \cdot \mathcal{H}f \cdot \mathbf{n} \\ &\quad + \cancel{\mathbf{n}^T \cdot \nabla \mathbf{n}} \cdot \mathbf{n} \mathbf{n}^T \cdot \nabla f + \cancel{\mathbf{n}^T \cdot \nabla \mathbf{n}} \cdot \nabla f \\ &= \Delta f - h(\mathbf{n} \cdot \nabla f) - \mathbf{n}^T \cdot \mathcal{H}f \cdot \mathbf{n}. \end{aligned} \quad (\text{A.13})$$

where  $\Delta$  denotes the Laplacian and  $\mathcal{H}$  denotes the Hessian operators respectively. As of  $h$ , it represents the mean curvature.

### A.3 Shape-gradient derivations of volume and area

Let us prove the expressions Eq.(2.7) and Eq.(2.8) from chapter 2. We start by the shape-gradient derivation of the volume:

$$V := \int_{\mathcal{V}} dV \quad (\text{A.14})$$

Thus, making use of the transport theorem for volume integrated functionals Eq.(A.5):

$$\begin{aligned} \delta V &= \int_S d\mathbf{x}^2 (\delta \mathbf{x} \cdot \mathbf{n}) 1 + \int_{\mathcal{V}} d\mathbf{x}^3 \delta 1 \\ &= \int_S d\mathbf{x}^2 (\delta \mathbf{x} \cdot \mathbf{n}). \end{aligned} \quad (\text{A.15})$$

As of Eq.(2.8):

$$A := \int_S dS. \quad (\text{A.16})$$

Therefore, using the second transport theorem Eq.(A.10):

$$\begin{aligned} \delta A &= \int_S d\mathbf{x}^2 \{ \delta 1 + (\mathbf{n} \cdot \nabla 1 + 2H 1) (\delta \mathbf{x} \cdot \mathbf{n}) \} \\ &= \int_S d\mathbf{x}^2 2H(\delta \mathbf{x} \cdot \mathbf{n}). \end{aligned} \quad (\text{A.17})$$

Q.E.D.

## A.4 Derivation of the first variation of the magnetic action

We start from the definition of the action Eq.(3.1):

$$\mathcal{S} := \oint_C \mathbf{A} \cdot d\mathbf{l}. \quad (\text{A.18})$$

Therefore,

$$\begin{aligned} \delta\mathcal{S} &= \oint_C \delta(\mathbf{A} \cdot d\mathbf{l}) \\ &= \oint_C (\delta\mathbf{A} \cdot d\mathbf{l} + \mathbf{A} \cdot \delta d\mathbf{l}) \\ &= \oint_C \left\{ (\delta\mathbf{x} \cdot \nabla) \mathbf{A} \cdot \mathbf{x}' + \mathbf{A} \cdot \delta\mathbf{x}' \right\} d\ell, \end{aligned} \quad (\text{A.19})$$

where  $f' = df/d\ell$ . Using the boundary conditions  $\mathbf{A} \cdot \delta\mathbf{x} = 0$  and integrating by parts,

$$\begin{aligned} \delta\mathcal{S} &= \oint_C (\delta\mathbf{x} \cdot \nabla) \mathbf{A} \cdot \mathbf{x}' - \mathbf{A}' \cdot \delta\mathbf{x} d\ell \\ &= \oint_C (\delta\mathbf{x} \cdot \nabla) \mathbf{A} \cdot \mathbf{x}' - \mathbf{x}' \cdot \nabla\mathbf{A} \cdot \delta\mathbf{x} d\ell \\ &= \oint_C \delta\mathbf{x} \cdot \mathbf{x}' \times (\nabla \times \mathbf{A}) d\ell \\ &= \oint_C (\mathbf{x}' \times \mathbf{B}) \cdot \delta\mathbf{x} d\ell, \end{aligned} \quad (\text{A.20})$$

Q.E.D.

## A.5 Frenet-Serret frame

In this section, we recall the definition and some properties of the well-known Frenet-Serret frame. The latter is defined as a basis of the three dimensional space, with the vectors  $\{\mathbf{t}, \mathbf{n}, \mathbf{b}\}$  for the tangent, normal and binormal vectors respectively, evaluated at some point along a curve. Fig.(A.1) represents the vectors  $\{\mathbf{t}, \mathbf{n}, \mathbf{b}\}$  at one point along a magnetic field line.

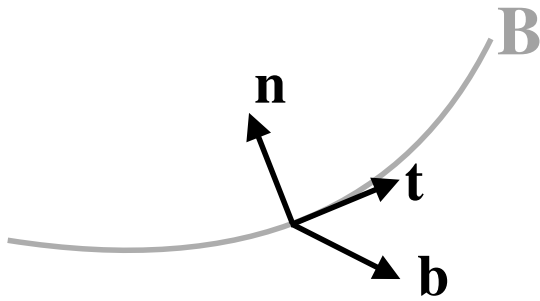


Figure A.1 – Frenet-Serret frame evaluated at a point on a  $\mathbf{B}$ -field line.

The vectors of the basis are orthonormal, and related to each other by mean of the curvature  $\kappa$  and the torsion  $\tau$  of the curve (field-line), through the following equations:

$$\begin{aligned} \frac{d\mathbf{t}}{ds} &= \kappa \mathbf{n} \\ \frac{d\mathbf{n}}{ds} &= -\kappa \mathbf{n} + \tau \mathbf{b} \\ \frac{d\mathbf{b}}{ds} &= -\tau \mathbf{n}, \end{aligned} \tag{A.21}$$

where  $s$  is the arc-length along the curve. The above torsion and curvature are the ones used in section 3.3.

## A.6 Vector Jacobian products

The gradient of the energy is implemented computing the derivatives of the energy with respect to the classes *field* and *coil*, and those derivatives are passed as arguments of the VJP functions of the field and coils. Since the *coil* class is made of the two subclasses *curve* and *current*, the energy has to be differentiated with respect to the constituent classes of the coils, as the derivative of a function composition.

$$\begin{aligned}\mathcal{E} &= \frac{1}{2} \sum_i I_i \oint_{C_i} \mathbf{A}(\boldsymbol{\Gamma}) \cdot d\mathbf{l} \\ &= \frac{1}{2} \sum_i I_i \oint_{C_i} \mathbf{A}(\boldsymbol{\Gamma}) \cdot \boldsymbol{\Gamma}' dl\end{aligned}\tag{A.22}$$

Thus,

$$\nabla_{\boldsymbol{\Gamma}'} \mathcal{E} := \frac{1}{2} \sum_i I_i \oint_{C_i} \mathbf{A}(\boldsymbol{\Gamma}) dl\tag{A.23}$$

$$\nabla_{\mathbf{A}} \mathcal{E} := \frac{1}{2} \sum_i \oint_{C_i} I_i d\mathbf{l}\tag{A.24}$$

$$\nabla_{\boldsymbol{\Gamma}} \mathcal{E} := \frac{1}{2} \sum_i I_i \oint_{C_i} J_{\mathbf{A}}(\boldsymbol{\Gamma}) \cdot \boldsymbol{\Gamma}' dl\tag{A.25}$$

$$\frac{\partial \mathcal{E}}{\partial I_i} = \frac{1}{2} \sum_i \oint_{C_i} \mathbf{A}(\mathbf{x}) \cdot d\mathbf{l}\tag{A.26}$$

Therefore, the total derivative of the energy with respect to the degrees of freedom reads:

$$\text{field.vjp}(\nabla_{\mathbf{A}} \mathcal{E}) + \sum_i \text{coil}_i.\text{vjp}(\nabla_{\boldsymbol{\Gamma}} \mathcal{E}, \nabla_{\boldsymbol{\Gamma}'} \mathcal{E}, \frac{\partial \mathcal{E}}{\partial I_i})\tag{A.27}$$

# Bibliography

- Baillod, A. (2023). Equilibrium pressure limits in stellarators. page 221.
- Boozer, A. H. (1998). What is a stellarator? *Physics of Plasmas*, 5(5):1647–1655.
- Byrd, R., Lu, P., Nocedal, J., and Zhu, C. (1995). A limited memory algorithm for bound constrained optimization. *SIAM Journal on Scientific Computing*, 16:1190–1208.
- Delfour, M. C. and Zolésio, J. P. (2011). *Shapes and Geometries*. Society for Industrial and Applied Mathematics, second edition.
- Duignan, N. and Meiss, J. D. (2021). Normal forms and near-axis expansions for beltrami magnetic fields. *Physics of Plasmas*, 28(12):122501.
- Floquet, G. (1883). Sur les équations différentielles linéaires à coefficients périodiques. *Annales scientifiques de l'École Normale Supérieure*, 2e série, 12:47–88.
- Greene, J. M. (2008). A method for determining a stochastic transition. *Journal of Mathematical Physics*, 20(6):1183–1201.
- Hanson, J. D. (2015). The virtual-casing principle and helmholtz's theorem. *Plasma Physics and Controlled Fusion*, 57(11):115006.
- Hudson, S. and Dewar, R. (2009). Are ghost surfaces quadratic-flux-minimizing? *Physics Letters A*, 373(48):4409–4415.
- Hudson, S. R. and Suzuki, Y. (2014). Chaotic coordinates for the Large Helical Device. *Physics of Plasmas*, 21(10):102505.
- Imbert-Gerard, L.-M., Paul, E. J., and Wright, A. M. (2020). An introduction to stellarators: From magnetic fields to symmetries and optimization.
- Klinger, T., Andreeva, T., Bozhenkov, S., Brandt, C., Burhenn, R., Buttenschön, B., Fuchert, G., Geiger, B., Grulke, O., Laqua, H., Pablant, N., Rahbarnia, K., Stange, T., von Stechow, A., Tamura, N., Thomsen, H., Turkin, Y., Wegner, T., Abramovic,

## Appendix A. Bibliography

---

I., Äkäslompolo, S., Alcusion, J., Aleynikov, P., Aleynikova, K., Ali, A., Alonso, A., Anda, G., Ascasibar, E., Bähner, J., Baek, S., Balden, M., Baldzuhn, J., Banduch, M., Barbui, T., Behr, W., Beidler, C., Benndorf, A., Biedermann, C., Biel, W., Blackwell, B., Blanco, E., Blatzheim, M., Ballinger, S., Bluhm, T., Böckenhoff, D., Böswirth, B., Böttger, L.-G., Borchardt, M., Borsuk, V., Boscary, J., Bosch, H.-S., Beurskens, M., Brakel, R., Brand, H., Bräuer, T., Braune, H., Brezinsek, S., Brunner, K.-J., Bussiahn, R., Bykov, V., Cai, J., Calvo, I., Cannas, B., Cappa, A., Carls, A., Carralero, D., Carraro, L., Carvalho, B., Castejon, F., Charl, A., Chaudhary, N., Chauvin, D., Chernyshev, F., Cianciosa, M., Citarella, R., Claps, G., Coenen, J., Cole, M., Cole, M., Cordella, F., Cseh, G., Czarnecka, A., Czerski, K., Czerwinski, M., Czymek, G., da Molin, A., da Silva, A., Damm, H., de la Pena, A., Degenkolbe, S., Dhard, C., Dibon, M., Dinklage, A., Dittmar, T., Drevlak, M., Drewelow, P., Drews, P., Durodie, F., Edlund, E., van Eeten, P., Effenberg, F., Ehrke, G., Elgeti, S., Endler, M., Ennis, D., Esteban, H., Estrada, T., Fellinger, J., Feng, Y., Flom, E., Fernandes, H., Fietz, W., Figacz, W., Fontdecaba, J., Ford, O., Fornal, T., Frerichs, H., Freund, A., Funaba, T., Galkowski, A., Gantenbein, G., Gao, Y., Regaña, J. G., Gates, D., Geiger, J., Giannella, V., Gogoleva, A., Goncalves, B., Goriaev, A., Gradic, D., Grahl, M., Green, J., Greuner, H., Grosman, A., Grote, H., Gruca, M., Guerard, C., Hacker, P., Han, X., Harris, J., Hartmann, D., Hathiramani, D., Hein, B., Heinemann, B., Helander, P., Henneberg, S., Henkel, M., Sanchez, J. H., Hidalgo, C., Hirsch, M., Hollfeld, K., Höfel, U., Höltig, A., Höschen, D., Houry, M., Howard, J., Huang, X., Huang, Z., Hubeny, M., Huber, M., Hunger, H., Ida, K., Ilkei, T., Illy, S., Israeli, B., Jablonski, S., Jakubowski, M., Jelonnek, J., Jenzsch, H., Jesche, T., Jia, M., Junghanns, P., Kacmarczyk, J., Kallmeyer, J.-P., Kamionka, U., Kasahara, H., Kasperek, W., Kazakov, Y., Kenmochi, N., Killer, C., Kirschner, A., Kleiber, R., Knauer, J., Knaup, M., Knieps, A., Kobarg, T., Kocsis, G., Köchl, F., Kolesnichenko, Y., Könies, A., König, R., Kornejew, P., Koschinsky, J.-P., Köster, F., Krämer, M., Krampitz, R., Krämer-Flecken, A., Krawczyk, N., Kremeyer, T., Krom, J., Krychowiak, M., Ksiazek, I., Kubkowska, M., Kühner, G., Kurki-Suonio, T., Kurz, P., Kwak, S., Landreman, M., Lang, P., Lang, R., Langenberg, A., Langish, S., Laqua, H., Laube, R., Lazerson, S., Lechte, C., Lennartz, M., Leonhardt, W., Li, C., Li, C., Li, Y., Liang, Y., Linsmeier, C., Liu, S., Lobsien, J.-F., Loesser, D., Cisquella, J. L., Lore, J., Lorenz, A., Losert, M., Lücke, A., Lumsdaine, A., Lutsenko, V., Maaßberg, H., Marchuk, O., Matthew, J., Marsen, S., Marushchenko, M., Masuzaki, S., Maurer, D., Mayer, M., McCarthy, K., McNeely, P., Meier, A., Mellein, D., Mendelevitch, B., Mertens, P., Mikkelsen, D., Mishchenko, A., Missal, B., Mittelstaedt, J., Mizuuchi, T., Mollen, A., Moncada, V., Mönnich, T., Morisaki, T., Moseev, D., Murakami, S., Náfrádi, G., Nagel, M., Naujoks, D., Neilson, H., Neu, R., Neubauer, O., Neuner, U., Ngo, T., Nicolai, D., Nielsen, S., Niemann, H., Nishizawa, T., Nocentini, R., Nührenberg, C., Nührenberg, J., Obermayer, S., Offermanns, G., Ogawa, K., Ölmanns, J., Ongena, J., Oosterbeek, J., Orozco, G., Otte, M., Rodriguez, L. P., Panadero, N., Alvarez, N. P., Papenfuß, D., Paqay, S., Pasch, E., Pavone, A., Pawelec, E., Pedersen, T., Pelka, G., Perseo, V.,

---

Peterson, B., Pilopp, D., Pingel, S., Pisano, F., Plaum, B., Plunk, G., Pölöskei, P., Porkolab, M., Proll, J., Puiatti, M.-E., Sitjes, A. P., Purps, F., Rack, M., Récsei, S., Reiman, A., Reimold, F., Reiter, D., Remppel, F., Renard, S., Riedl, R., Riemann, J., Risse, K., Rohde, V., Röhlinger, H., Romé, M., Rondeshagen, D., Rong, P., Roth, B., Rudischhauser, L., Rummel, K., Rummel, T., Runov, A., Rust, N., Ryc, L., Ryosuke, S., Sakamoto, R., Salewski, M., Samartsev, A., Sanchez, E., Sano, F., Satake, S., Schacht, J., Satheeswaran, G., Schauer, F., Scherer, T., Schilling, J., Schlaich, A., Schlisio, G., Schluck, F., Schlüter, K.-H., Schmitt, J., Schmitz, H., Schmitz, O., Schmuck, S., Schneider, M., Schneider, W., Scholz, P., Schrittwieser, R., Schröder, M., Schröder, T., Schroeder, R., Schumacher, H., Schweer, B., Scott, E., Sereda, S., Shanahan, B., Sibilia, M., Sinha, P., Sipliä, S., Slaby, C., Slezczka, M., Smith, H., Spiess, W., Spong, D., Spring, A., Stadler, R., Stejner, M., Stephey, L., Stridde, U., Suzuki, C., Svensson, J., Szabó, V., Szabolics, T., Szepesi, T., Szökefalvi-Nagy, Z., Tancetti, A., Terry, J., Thomas, J., Thumm, M., Travere, J., Traverso, P., Tretter, J., Mora, H. T., Tsuchiya, H., Tsujimura, T., Tulipán, S., Unterberg, B., Vakulchyk, I., Valet, S., Vano, L., van Milligen, B., van Vuuren, A., Vela, L., Velasco, J.-L., Vergote, M., Vervier, M., Vianello, N., Viebke, H., Vilbrandt, R., Vorköper, A., Wadle, S., Wagner, F., Wang, E., Wang, N., Wang, Z., Warmer, F., Wauters, T., Wegener, L., Weggen, J., Wei, Y., Weir, G., Wendorf, J., Wenzel, U., Werner, A., White, A., Wiegel, B., Wilde, F., Windisch, T., Winkler, M., Winter, A., Winters, V., Wolf, S., Wolf, R., Wright, A., Wurden, G., Xanthopoulos, P., Yamada, H., Yamada, I., Yasuhara, R., Yokoyama, M., Zanini, M., Zarnstorff, M., Zeitler, A., Zhang, D., Zhang, H., Zhu, J., Zilker, M., Zocco, A., Zoleznik, S., and Zuin, M. (2019). Overview of first wendelstein 7-x high-performance operation. *Nuclear Fusion*, 59(11):112004.

Landreman, M. (2022). Mapping the space of quasisymmetric stellarators using optimized near-axis expansion. *Journal of Plasma Physics*, 88(6).

Landreman, M., Hurwitz, S., and Antonsen, T. (2023). Efficient calculation of internal magnetic field and self-force for electromagnetic coils. Invited talk.

Landreman, M., Medasani, B., Wechsung, F., Giuliani, A., Jorge, R., and Zhu, C. (2021). Simsoft: A flexible framework for stellarator optimization. *Journal of Open Source Software*, 6(65):3525.

Landreman, M. and Paul, E. (2022). Magnetic fields with precise quasisymmetry for plasma confinement. *Physical Review Letters*, 128(3).

Laurain, A. and Sturm, K. (2015). Distributed shape derivative via averaged adjoint method and applications.

Li, S., Jiang, H., Ren, Z., and Xu, C. (2014). Optimal Tracking for a Divergent-Type Parabolic PDE System in Current Profile Control. *Abstract and Applied Analysis*, 2014(SI13):1 – 8.

## Appendix A. Bibliography

---

- Lumsdaine, A., Bjorholm, T., Harris, J., McGinnis, D., Lore, J. D., Boscary, J., Tretter, J., Clark, E., Ekici, K., Fellinger, J., Hölbe, H., Neilson, H., Titus, P., and Wurden, G. A. (2016). Overview of design and analysis activities for the w7-x scraper element. *IEEE Transactions on Plasma Science*, 44(9):1738–1744.
- Mackay, R. and Meiss, J. (1983). Linear stability of periodic orbits in lagrangian systems. *Physics Letters A*, 98(3):92–94.
- Magnus, W. (1953). *Infinite Determinants in the Theory of Mathieu's and Hill's Equations*, volume 1. Mathematics Research Group, Washington Square College of Arts and Science . . . .
- Meiss, J. (2007). *Differential Dynamical Systems*. SIAM.
- Mercier, C., Euratom, and of the European Communities, C. (1987). *Lectures in Plasma Physics: The Magnetohydrodynamic Approach to Plasma Confinement in Closed Magnetic Configurations*. EUR 5127 EN/1987. Commission of the European Communities.
- Molinari, L. G. (2008). Determinants of block tridiagonal matrices. *Linear Algebra and its Applications*, 429(8-9):2221–2226.
- Nies, R., Paul, E. J., Hudson, S. R., and Bhattacharjee, A. (2022). Adjoint methods for quasi-symmetry of vacuum fields on a surface. *Journal of Plasma Physics*, 88(1).
- Peitgen, H.-O. and Saupe, D., editors (1988). *The Science of Fractal Images*. Springer-Verlag, Berlin, Heidelberg.
- Solovev, L. S. and Shafranov, V. D. (1970). Reviews of plasma physics. volume 5.
- TODOROKI, J. (2003). Calculating Rotational Transform Following Field Lines. *Journal of Plasma and Fusion Research*, 79(4):321–322.
- Z. X. Wang, D. R. Guo, X. J. X. (1989). *Special Functions*. World Scientific Pub Co Inc.
- Zhu, C., Byrd, R. H., Lu, P., and Nocedal, J. (1997). Algorithm 778: L-bfgs-b: Fortran subroutines for large-scale bound-constrained optimization. *ACM Trans. Math. Softw.*, 23(4):550–560.